Inhibition of perforin binding activity by surface membrane proteins. *J Immunol* **144**, 998–1003.

Kuzushima, K., Hayashi, N., Kimura, H. & Tsurumi, T. (2001). Efficient identification of HLA-A*2402-restricted cytomegalovirus-specific $CD8^+$ T-cell epitopes by a computer algorithm and an enzyme-linked immunospot assay. *Blood* **98**, 1872–1881.

Lehmann, C., Zeis, M., Schmitz, N. & Uharek, L. (2000). Impaired binding of perforin on the surface of tumor cells is a cause of target cell resistance against cytotoxic effector cells. *Blood* **96**, 594–600.

Lemasson, I., Lewis, M. R., Polakowski, N., Hivin, P., Cavanagh, M. H., Thébault, S., Barbeau, B., Nyborg, J. K. & Mesnard, J. M. (2007). HTLV-1 bZIP protein interacts with the cellular transcription factor CREB to inhibit HTLV-1 transcription. *J Virol* **81**, 1543–1553.

Muller, C. & Tschopp, J. (1994). Resistance of CTL to perforin-mediated lysis. Evidence for a lymphocyte membrane protein interacting with perforin. *J Immunol* **153**, 2470–2478.

Odeberg, J., Browne, H., Metkar, S., Froelich, C. J., Brandén, L., Cosman, D. & Söderberg-Nauclér, C. (2003). The human cytomegalovirus protein UL16 mediates increased resistance to natural killer cell cytotoxicity through resistance to cytolytic proteins. *J Virol* **77**, 4539–4545.

Ohminami, H., Yasukawa, M. & Fujita, S. (2000). HLA class I-restricted lysis of leukemia cells by a $CD8^+$ cytotoxic T-lymphocyte specific for WT1 peptide. *Blood* **95**, 286–293.

Satou, Y. & Matsuoka, M. (2007). Implication of the *HTLV-I bZIP factor* gene in the leukemogenesis of adult T-cell leukemia. *Int J Hematol* **86**, 107–112.

Satou, Y., Yasunaga, J., Yoshida, M. & Matsuoka, M. (2006). *HTLV-I basic leucine zipper factor gene* mRNA supports proliferation of adult T cell leukemia cells. *Proc Natl Acad Sci U S A* **103**, 720–725.

Suemori, K., Fujiwara, H., Ochi, T., Azuma, T., Yamanouchi, J., Narumi, H., Yakushijin, Y., Hato, T., Hasegawa, H. & Yasukawa, M. (2008). Identification of an epitope derived from CML66, a novel tumor-associated antigen broadly expressed in human leukemia, recognized by HLA-A*2402-restricted cytotoxic T lymphocytes. *Cancer Sci* **99**, 1414–1419.

Taylor, G. P. & Matsuoka, M. (2005). Natural history of adult T-cell leukemia/lymphoma and approaches to therapy. *Oncogene* **24**, 6047–6057.

Utsunomiya, A., Miyazaki, Y., Takatsuka, Y., Hanada, S., Uozumi, K., Yashiki, S., Tara, M., Kawano, F., Saburi, Y. & other authors (2001). Improved outcome of adult T cell leukemia/lymphoma with allogeneic hematopoietic stem cell transplantation. *Bone Marrow Transplant* **27**, 15–20.

Yasukawa, M., Ohminami, H., Yakushijin, Y., Arai, J., Hasegawa, A., Ishida, Y. & Fujita, S. (1999). Fas-independent cytotoxicity mediated by human $CD4^+$ CTL directed against herpes simplex virus-infected cells. *J Immunol* **162**, 6100–6106.

Int J Hematol (2009) 90:537–539
DOI 10.1007/s12185-009-0430-2

LETTER TO THE EDITOR

Compound heterozygous mutations in the *PROS1* gene responsible for quantitative and qualitative protein S deficiency

Jun Yamanouchi · Takaaki Hato · Tatsushiro Tamura · Hiroshi Fujiwara · Yoshihiro Yakushijin · Masaki Yasukawa

Received: 12 May 2009 / Revised: 2 September 2009 / Accepted: 6 September 2009 / Published online: 14 October 2009

Protein S (PS) is a vitamin K-dependent plasma glycoprotein, which plays an important role in the blood anticoagulant system. The PS gene (*PROS1*) spans some 80 kb of genomic DNA, composed of 15 exons and 14 introns, and is closely linked to a highly homologous pseudogene (*PROS2*), whose sequence is 96% identical to that of *PROS1* [1]. Congenital PS deficiency caused by *PROS1* mutations is associated with an increased risk of thromboembolic disease. In this study, we investigated the molecular basis of a patient with both quantitative and qualitative PS deficiency.

A 69-year-old man had a medical examination in our hospital because of progressive bilateral leg pain and swelling. He was diagnosed with deep vein thrombosis (DVT) based on the venographs of the legs. Laboratory tests showed normal values of platelet count, prothrombin time, activated partial thromboplastin time, ATIII activity and protein C activity. Test results for lupus anticoagulant and anti-cardiolipin β2GPI antibody were negative. Total PS antigen, free-PS antigen and PS activity levels were 49.0% (normal range 65–135%), 26.7% (60–150%) and 10% (60–150%), respectively. From these findings, he was diagnosed as having PS deficiency.

J. Yamanouchi · T. Hato · T. Tamura · H. Fujiwara · Y. Yakushijin · M. Yasukawa
Departments of Bioregulatory Medicine and Blood Transfusion and Cell Therapy, Ehime University Graduate School of Medicine, Toon, Ehime, Japan

J. Yamanouchi (✉)
Department of Bioregulatory Medicine, Ehime University Graduate School of Medicine, Shitsukawa, Toon, Ehime 791-0295, Japan
e-mail: yamanouc@m.ehime-u.ac.jp

To define causative mutation(s) of *PROS1*, genomic DNA was isolated from peripheral blood leukocytes of the patient and his family members. This study was approved by the Ethics Committee of Ehime University Graduate School of Medicine. All subjects gave their written informed consent. We amplified each of 15 exons including the exon/intron boundaries of the *PROS1* by a polymerase chain reaction (PCR), and their PCR products were directly sequenced. We identified a heterozygous transition of A–G at nucleotide 586, which resulted in Lys196 being replaced by Glu (K196E mutation; adopted from the numbering standards of the Nomenclature Working Group, wherein the 'A' of the ATG-translation initiation codon is numbered as 1 for nucleotides, and the initial methionine is numbered as 1 for amino acids [2]). The K196E mutation has been reported to be a polymorphism in the Japanese population formerly known as PS Tokushima that was previously referred to as the K155E mutation. This mutation was originally identified in a Japanese patient with PS deficiency suffering from DVT, and the PS activity was decreased in carriers of the K196E mutation with normal PS levels [3]. However, the results regarding plasma PS activity in individuals with this mutation remained controversial. Another study found PS activity within the normal range in affected individuals [4]. A recent analysis of the recombinant mutant protein demonstrated that the antigen level of K196E was normal and its activity was reduced to 60–70% [5]. However, the PS activity in our patient was very low (10%), suggesting that the patient's PS deficiency was not simply explained by the K196E mutation. Thus, we reviewed the results of the sequence analysis of the *PROS1*, and noticed that a certain region of *PROS1* (the C-terminal of exon 14) was not analyzed because the presence of *PROS2* disturbs to set up the PCR primer suitable for amplification of this region of *PROS1*.

To determine the sequence of this region, we obtained the messenger RNA (mRNA) from the patient's blood platelets and tested a RT-PCR. We found a heterozygous transition of A–G at nucleotide 1849, which resulted in Thr617 being replaced by Ala (T617A mutation). Subcloning of the RT-PCR products encompassing the T617A and K196E mutations into TA vectors showed that all the products had either mutation, but not both, suggesting that these two mutations are located on the different allele.

The T617A was a novel mutation and was unlikely to constitute a polymorphism because this mutation was not found in a recent analysis of 173 patients with DVT [6]. We characterized this mutant protein. PS cDNAs with T617A or K196E mutation were generated from a wild-type human PS cDNA (a generous gift from Dr. K. Suzuki, University of Mie, Japan). The recombinant PS protein was stably expressed in human embryo kidney 293 cells in the presence of vitamin K. Recombinant PS proteins synthesized in the cells and secreted into the culture supernatant were analyzed by Western blotting (Fig. 1). The PS proteins were secreted into the culture supernatants of the cells expressing wild type and K196E. In contrast, no PS secretion was observed in the T617A mutant. However, the cell lysate of the T617A mutant contained the PS protein as well as those of wild type and K196E mutants, suggesting that the T617A mutation impairs secretion of the PS protein. The ELISA for recombinant PS antigens confirmed the results of blotting (0 and 70% of wild type in the supernatants of T617A and K196E; 76.8 and 78% of wild type in the cell lysates of T617A and K196E, respectively). These results, together with previous findings of K196E, suggest that the K196E/T617A double mutation in the *PROS1* is responsible for the moderate decrease in PS antigen and disproportional reduction in PS activity in this patient.

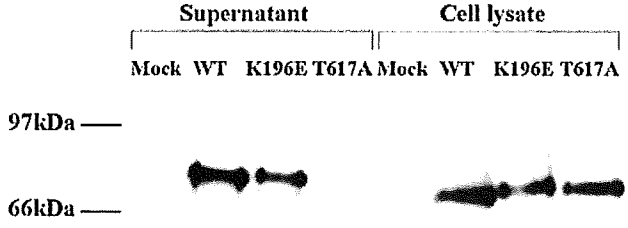

Fig. 1 Expression of recombinant PS. Intracellular and secreted recombinant PS were detected by Western blotting with a sheep anti-human PS antibody (AbD Serotec, Oxford, UK) followed by HRP-conjugated anti-sheep IgG and streptavidin-HRP

We next explored the *PROS1* from the patient's family (Fig. 2). The patient (III-2) had a consanguineous marriage and the patient's oldest son (IV-1) was found to have the same double mutation as the patient. His PS antigen (free 42%, total 82%) and activity (15%) were also similar to the patient's values, but he had no episode of thrombosis at present. The other seven family members (III-1, III-3, IV-2, IV-3, IV-4, V-1, V-2) who have K196E, but not T617A, showed normal levels of PS antigen with slightly decreased normal levels of PS activity. These results are consistent with the in vitro characterization of the K196E/T617A mutations.

The T617 residue lies within the sex hormone-binding globulin-like domain of the PS protein. This domain mediates the binding of PS to a complement-regulator component, C4b-binding protein. Many of mutations within this domain have been reported to result in a type-I PS deficiency [7]. Our in vitro result with T617A suggests that the single T617A mutation may also cause type-I PS

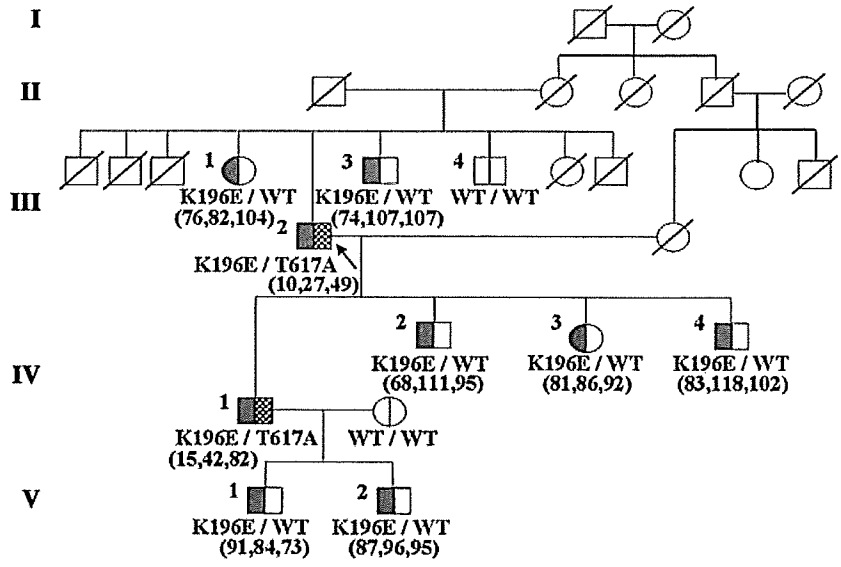

Fig. 2 Family pedigree. The *arrow* indicates the proband. ⊠: deceased. The *numbers* in the *parentheses* are expressed in the order of PS activity (%), free-PS antigen (%) and total PS antigen (%). The concentrations of total and free-PS antigens were measured by enzyme-linked immunosorbent assay and PS activity was determined on the basis of a clotting assay

deficiency due to impairment of PS secretion. Because T617 is a highly conserved residue among species including, rabbit, porcine, bovine and monkey, it may be an essential structure element [8].

Our study demonstrates that the phenotype of the combination of quantitative and qualitative PS deficiency was brought about by compound heterozygous mutations in the *PROS1*. Such a double mutation should be considered as one of the molecular mechanism for patients with both quantitative and qualitative PS deficiency.

References

1. Schmidel DK, Tatro AV, Phelps LG, Tomczak JA, Long GL. Organization of the human protein S genes. Biochemistry. 1990;29:7845–52.
2. Antonarakis SE, and the Nomenclature Working Group. Recommendations for a nomenclature system for human gene mutations. Hum Mutat. 1998;11:1–3.
3. Hayashi T, Nishioka J, Shigekiyo T, Saito S, Suzuki K. Protein S Tokushima: abnormal molecule with a substitution of Glu for Lys-155 in the second epidermal growth factor-like domain of protein S. Blood. 1994;83:683–90.
4. Yamazaki T, Sugiura I, Matsushita T, Kojima T, Kagami K, Takamatsu J, et al. A phenotypically neutral dimorphism of protein S: the substitution of Lys155 by Glu in the second EGF domain predicted by an A to G base exchange in the gene. Thromb Res. 1993;70:395–403.
5. Tsuda H, Urata M, Tsuda T, Wakiyama M, Iida H, Nakahara M, et al. Four missense mutations identified in the protein S gene of thrombosis patients with protein S deficiency effects on secretion and anticoagulant activity of protein S. Thromb Res. 2002;105:233–9.
6. Miyata T, Sato Y, Ishikawa J, Okada H, Takeshita S, Sakata T, et al. Prevalence of genetic mutations in protein S, protein C and antithrombin genes in Japanese patients with deep vein thrombosis. Thromb Res. 2009;124:14–8.
7. Villoutreix BO, Dahlback B, Borgel D, Gandrille S, Muller YA. Three-dimensional model of the SHBG-like region of anticoagulant protein S: new structure-function insights. Proteins. 2001;43:203–16.
8. Greengard JS, Fernandez JA, Radtke K, Griffin JH. Identification of candidate residues for interaction of protein S with C4b binding protein and activated protein C. Biochem J. 1995;305:397–403.

Improved Expression and Reactivity of Transduced Tumor-Specific TCRs in Human Lymphocytes by Specific Silencing of Endogenous TCR

Sachiko Okamoto,[1] Junichi Mineno,[1] Hiroaki Ikeda,[2] Hiroshi Fujiwara,[3] Masaki Yasukawa,[3] Hiroshi Shiku,[2] and Ikunoshin Kato[1]

[1]Center for Cell and Gene Therapy, Takara Bio, Inc., Shiga, Japan; [2]Department of Immuno-Gene Therapy, Mie University Graduate School of Medicine, Mie, Japan; and [3]Department of Bioregulatory Medicine, Ehime University Graduate School of Medicine, Ehime, Japan

Abstract

Adoptive T-cell therapy using lymphocytes genetically engineered to express tumor antigen-specific TCRs is an attractive strategy for treating patients with malignancies. However, there are potential drawbacks to this strategy: mispairing of the introduced TCR α/β chains with the endogenous TCR subunits and competition of CD3 molecules between the introduced and endogenous TCRs can impair cell surface expression of the transduced TCR, resulting in insufficient function and potential generation of autoreactive T cells. In addition, the risk of tumor development following the infusion of cells with aberrant vector insertion sites increases with the vector copy number in the transduced cells. In this study, we developed retroviral vectors encoding both small interfering RNA constructs that specifically down-regulate endogenous TCR and a codon-optimized, small interfering RNA–resistant TCR specific for the human tumor antigens MAGE-A4 or WT1. At low copy numbers of the integrated vector, the transduced human lymphocytes exhibited high surface expression of the introduced tumor-specific TCR and reduced expression of endogenous TCRs. In consequence, the vector-transduced lymphocytes showed enhanced cytotoxic activity against antigen-expressing tumor cells. Therefore, our novel TCR gene therapy may open a new gate for effective immunotherapy in cancer patients. [Cancer Res 2009;69(23):9003–11]

Introduction

Several groups have shown that TCR gene transfer using retroviral vectors is an attractive strategy for redirecting the antigen specificity of polyclonal primary T cells to create tumor- or pathogen-specific lymphocytes (1–6). This approach has been suggested as a way to overcome the limitations of current adoptive T-cell therapies, which rely on the isolation and expansion of antigen-specific lymphocytes that preexist in the patient (7–10). Recently, clinical trials for the treatment of metastatic melanoma patients reported objective cancer regression in up to 30% of patients using autologous lymphocytes that were retrovirally transduced with melanoma/melanocyte antigen-specific TCRs (11, 12). These data suggest that adoptive cell therapy with TCR gene-modified lymphocytes is a promising approach for immunotherapy in cancer patients and encourage the development of novel TCR gene therapy approaches that result in improved antitumor activity.

However, the limited efficacy of TCR gene therapy has been reported to be associated with inefficient surface expression of transduced TCRs (13–16). The existence of the endogenous TCR is one of the major reasons for inefficient cell surface expression of the introduced TCR heterodimers. The introduced TCR α and β chains have been reported to mispair with the endogenous TCR chains, resulting in insufficient formation of the introduced TCR heterodimers (16–19). In addition, endogenous TCRs compete with the introduced TCRs for CD3 molecules (16–18, 20, 21). Because the stable cell surface expression of TCRs requires TCR assembly with CD3 γ, δ, ε, and ζ chains, this mechanism can also reduce the cell surface expression of the introduced TCR.

The expression level of the transgene can be enhanced by increasing the vector copy number in the transduced cells (22). However, it has been suggested that restricting the proviral copy number per cell decreases the number of potential vector insertions into sites that may promote proto-oncogene activation, tumor suppressor gene inactivation, or chromosomal instability (23, 24). A low copy number is ideal for reducing the risk of insertional mutagenesis even when using mature T cells instead of stem cells (22). Therefore, it is necessary to determine the efficacy of retroviral vectors based on the proviral copy number in transduced cells to precisely evaluate the usefulness and safety of each vector. Thus, a strategy for achieving high expression of transduced TCRs with relatively low copy numbers is required. Moreover, it has been suggested that the mispairing of introduced TCRs with endogenous TCRs may result in the generation of T cells with unexpected specificities, including self-reactive T cells (16–18, 25).

Recently, we isolated rearranged TCR α and β genes from a human $CD8^+$ T-cell clone that recognizes a tumor-specific antigen MAGE-A4–derived peptide in a HLA-A*2402–restricted manner. Polyclonal human lymphocytes retrovirally transduced with these TCR genes showed stable expression of the transgenes and specific cytotoxicity against MAGE-A4–expressing tumor cells (26, 27).

In this study, we determined whether we could induce high expression of MAGE-A4–specific TCRs and enhance the biological activity of transduced human lymphocytes at a low proviral copy number by combining small interfering RNA (siRNA) gene silencing of endogenous TCRs with siRNA-resistant, codon-optimized, transduced TCR genes. After normalizing the proviral copy number in the transduced cells, we evaluated the newly developed retroviral vectors for expression of transduced TCRs, inhibition of endogenous TCRs, and specific cytotoxicity against MAGE-A4–expressing tumor cells. The effectiveness of this approach was further determined for another TCR specific for WT1 tumor antigen.

Note: Supplementary data for this article are available at Cancer Research Online (http://cancerres.aacrjournals.org/).

Requests for reprints: Junichi Mineno, Center for Cell and Gene Therapy, Takara Bio Inc., SETA 3-4-1, Otsu, Shiga 520-2193, Japan. Phone: 81-77-543-7318; Fax: 81-77-543-2494; E-mail: minenoj@takara-bio.co.jp.

doi:10.1158/0008-5472.CAN-09-1450

Materials and Methods

Peripheral blood mononuclear cells. Peripheral blood mononuclear cells (PBMC) were isolated from healthy donors who gave their informed consent. PBMCs were cultured in GT-T503 (Takara Bio) supplemented with 1% autologous plasma, 0.2% HSA, 2.5 mg/mL fungizone (Bristol-Myers Squibb), and 600 IU/mL interleukin-2. The study was approved by the Ethics Committee of Takara Bio.

Cell lines for evaluating the specific inhibitory effects of siRNAs. The cDNAs of WT-MAGE-A4–specific TCR α and β chains with Cβ2 regions, codon-optimized TCR α and β chains, and WT-CEA-specific TCR β chain with a Cβ1 (28) region were individually cloned into the retroviral vector pMEI-5 (Takara Bio). VSVG-pseudotyped retroviruses were transiently obtained by conventional methods using HEK293T cells. HEK293 cells were transduced with VSVG-pseudotyped retroviruses and designated 293-A, 293-coA, 293-BC1, 293-BC2, and 293-coB. These HEK293 cell lines expressed WT-MAGE-A4–specific TCR α, codon-optimized MAGE-A4–specific TCR α, WT-CEA-specific TCR β, WT-MAGE-A4–specific TCR β and codon-optimized MAGE-A4–specific TCR β, respectively.

Construction of retroviral vectors and retroviral transduction. The sequences of TCR α and β cDNAs from the HLA-A*2402–restricted MAGE-A4–specific $CD8^+$ CTL clone 2-28 (26, 27) were codon-optimized by GeneArt. We designed the siRNA sequences targeting TCR-Cα and TCR-Cβ to be mismatched to codon-optimized sequences. C-optiTCR and MS-bPa (27) retroviral vectors encoded the codon-optimized MAGE-A4–specific TCR α/β (Fig. 1*A*) and WT-MAGE-A4–specific TCR α/β, respectively. The multigene-expressing retroviral vectors were constructed by cloning the pol III promoter-driven short hairpin RNA into the C-optiTCR plasmid. The cluster sequences of human primary microRNA (pri-miRNA) were cloned into the C-optiTCR plasmid in which the mature miRNA sequences had been replaced by siRNA sequences (Fig. 1*B* and *C*). The TCR genes of the HLA-A*2402–restricted $WT1_{235\text{-}243}$-specific $CD8^+$ CTL clone TAK-1 (29–31) were used to construct WT1-WT and WT1-CO retroviral vectors encoding wild-type and partially codon-optimized WT1-specific TCR α/β, respectively. Partial codon optimization was done by replacing the C_α and C_β regions with codon-optimized TCR C_α and C_β regions, respectively. The WT1-siTCR vector was also constructed by cloning the siRNA expression unit into the WT1-CO vector (Fig. 1*D*). PBMCs were stimulated with 30 ng/mL OKT-3 (Janssen Pharmaceutical) and 600 IU/mL interleukin-2 and transduced using the RetroNectin-bound Virus Infection Method in which retroviral solutions were preloaded onto RetroNectin (Takara Bio)–coated plates, centrifuged at 2,000 × *g* for 2 h, and rinsed with PBS. Cells were applied onto the preloaded plate.

Transfection of siRNAs and TCR RNA quantification. The double-stranded siRNAs (negative control siRNA 5′-CCAATTACGCGTTGGTAGC-3′, siRNA-a04 5′-GTAAGGATTCTGATGTGTA-3′, siRNA-b03 5′-CCAC-CATCCTCTATGAGAT-3′, siRNA-a06 5′-CAACAAATCTGACTTTGCA-3′, and siRNA-b02 5′-CCATGGTCAAGAGAAAGGA-3′) were introduced using TransIT-TKO (Mirus Bio) or a Human T-Cell Nucleofector kit (Amaxa). To quantify the TCR RNAs, quantitative reverse transcription-PCR was done using SYBR PrimeScript Reverse Transcription-PCR kit (Takara Bio) with primer sets specific for the WT or codon-optimized TCR C regions. Primers for human glyceraldehyde-3-phosphate dehydrogenase were used for normalization. Primers were as follows: human glyceraldehyde-3-phosphate dehydrogenase 5′-GCACCGTCAAGGCTGAGAAC-3′ and 5′-ATGGTGGT-GAA-GACGCCAGT-3′, endogenous TCR α 5′-GTGCAAACGCCTTCAACAA-CA-3′ and 5′-GACCAGCTTGACATCACAGGAAC-3′, endogenous TCR β 5′-GCCCTCAATGACTCCAGATAC-3′ and 5′-CCTGGGTCCACTCGTCATTC-3′, codon-optimized TCR α 5′-AGAGCTTCGAGACCGACACCA-3′ and

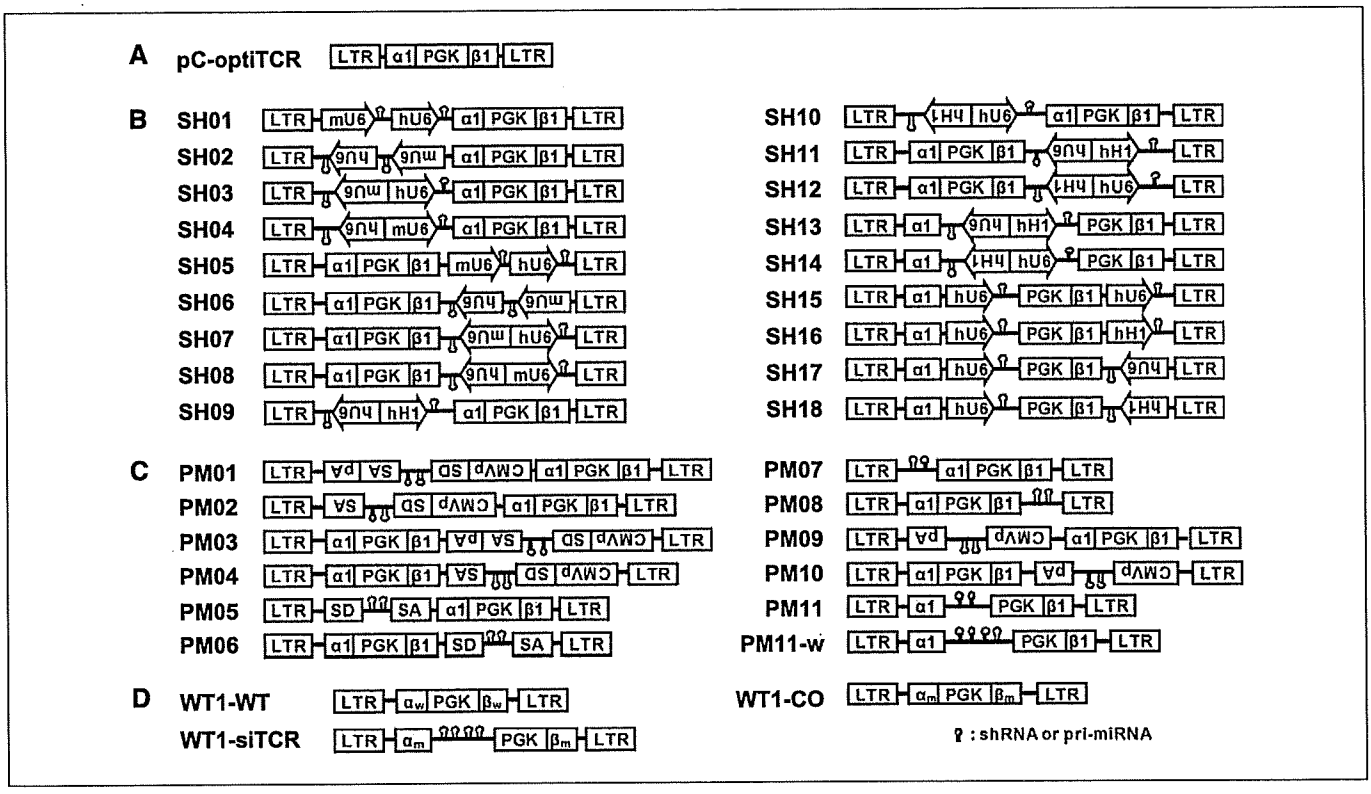

Figure 1. Retroviral vector construction in this study. *A*, retroviral vector pC-optiTCR. *B* and *C*, retroviral vectors that express siRNA as short hairpin RNA (*B*) or as a cluster sequence of pri-miRNA (*C*). *D*, retroviral vectors encoding WT1-specific TCR α/β and siRNAs. Construction of TCR gene expression retroviral vectors was described in the supplementary file. *α1*, codon-optimized MAGE-A4–specific TCR α chain; *β1*, codon-optimized MAGE-A4–specific TCR β chain; *PGK*, PGK promoter; *hU6*, human U6 promoter; *mU6*, mouse U6 promoter; *hH1*, human H1 promoter; *LTR*, long terminal repeat of MSCV; *CMVp*, cytomegalovirus promoter; *SD*, splicing donor; *SA*, splicing acceptor; *pA*, poly(A) signal sequence; α_w, wild type WT1-specific TCR α chain; β_w, wild type WT1-specific TCR β chain; α_m, partially codon-optimized WT1-specific TCR α chain; β_m, partially codon-optimized WT1-specific TCR β chain.

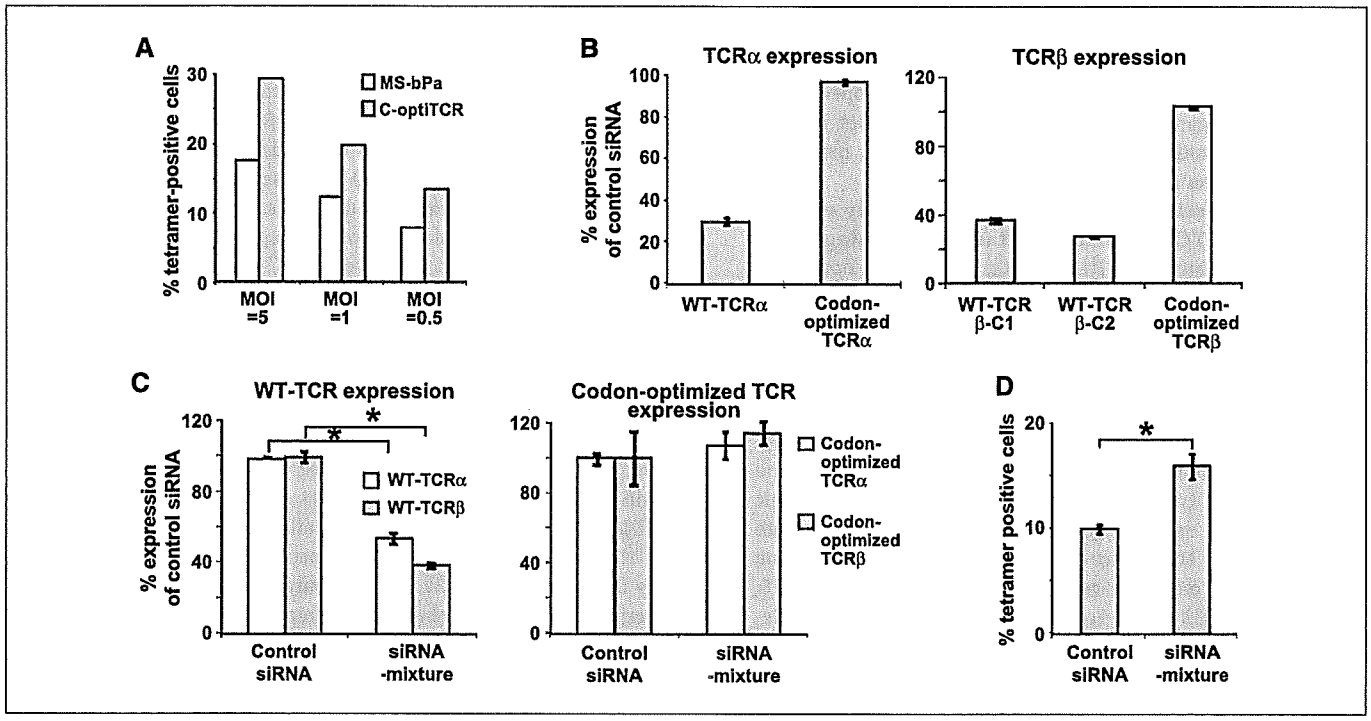

Figure 2. Improved expression of an ectopic TCR by codon optimization and the use of endogenous TCR α/β–specific siRNAs. *A*, activated PBMCs were transduced with MS-bPa or C-optiTCR retroviral vectors that expressed WT or codon-optimized TCR at indicated multiplicity of infection (*MOI*). Percentage of tetramer-positive cells among $CD8^+$ cells is indicated. Similar experiments were done using at least three donors' PBMCs with similar results. *B*, quantification of WT and codon-optimized TCR α mRNAs of siRNA-a04–transfected 293-A and 293-coA cells that express WT and codon-optimized TCR α, respectively (*left*). Quantification of WT-TCR βC1 and βC2 and codon-optimized TCR β mRNAs of siRNA-b03–transfected 293-BC1, 293-BC2, and 293-coB cells that express WT-TCR βC1, WT-TCR βC2, and codon-optimized TCR β, respectively (*right*). Each TCR expression is indicated as a percentage of negative control siRNA-transfected cells. Representative of three independent experiments. *C* and *D*, activated PBMCs were transduced with the C-optiTCR retroviral vector, and negative control siRNA or the siRNA mixture (siRNA-a04 + siRNA-b03) was transfected by electroporation. Quantification of WT-TCR α/β (*C, left*) and ectopic codon-optimized TCR α/β (*C, right*). Representative of three independent experiments. Percentage of tetramer-positive cells among $CD8^+$ cells (*D*). These experiments were done using two donors' PBMCs with similar results. *, $P < 0.05$.

5′-TGAAGCCGGCCACTTTCAG-3′, and codon-optimized TCR β 5′-GGCTTCACCAGCGAGAGCTA-3′ and 5′-TCACCATGGCCATCAGCA-3′.

Flow cytometric analysis. PE-conjugated anti-human TCR α/β monoclonal antibody (mAb; BD Pharmingen), FITC-conjugated anti-CD8 mAb (Becton Dickinson), FITC-conjugated anti-human TCR Vβ2, Vβ3, and Vβ17 mAbs (Beckman Coulter), PE-conjugated MAGE-$A4_{143\text{-}151}$/HLA-A*2402 tetramer (provided from Ludwig Institute for Cancer Research), and PE-conjugated $WT1_{235\text{-}243}$/HLA-A*2402 tetramer (provided by Dr. Kuzushima, Aichi Cancer Center Research Institute) were used. Stained cells were analyzed using Cytomics (Beckman Coulter) or FACS CantoII (Becton Dickinson).

Measurement of proviral copy number of retrovirus-transduced PBMCs. Genomic DNA was purified from transduced PBMCs, and the average proviral copy number per cell was quantified using the Cycleave PCR Core kit (Takara Bio) and the Proviral Copy Number Detection Primer Set (Takara Bio).

Calcein-AM cytotoxicity assay. The ability of the transduced PBMCs to lyse targets was measured using a calcein-AM (Dojindo) release assay as described previously (32).

Statistics. Student's *t* test was used for comparison of the means. *P* values < 0.05 were considered statistically significant.

Results

Codon-optimized TCR α and β cDNA and endogenous TCR α/β–specific siRNAs improve the expression of the introduced TCR. Previously, we reported that genetic engineering of PBMCs using a retroviral vector MS-bPa that encodes MAGE-$A4_{143\text{-}151}$–specific TCR α/β chains generated MAGE-A4–specific $CD8^+$ T cells (26, 27). In the current study, we initially investigated the effect of codon optimization on the expression level of the MAGE-$A4_{143\text{-}151}$–specific TCR by adapting the codon usage to the codon bias of *Homo sapiens* genes and avoiding *cis*-acting sequence motifs such as splice donor sites. The codon-optimized TCR α and β cDNAs were cloned into the retroviral vector and designated C-optiTCR (Fig. 1*A*). Codon optimization improved the expression of the MAGE-A4–specific TCR on the surface when compared with T cells transduced with MAGE-A4–specific WT-TCR (Fig. 2*A*) in agreement with previous reports (15, 33). Next, we designed several siRNAs specific for the TCR C_α region or the TCR $C_\beta1/C_\beta2$ regions to suppress only the endogenous WT-TCR α/β. We selected the best siRNAs based on their gene suppression efficiencies (data not shown). The selected siRNAs, siRNA-a04 and siRNA-b03, specifically inhibited the WT-TCR α and β genes but did not alter the expression of the codon-optimized TCR α or β (Fig. 2*B*). Finally, we confirmed that the combination of codon optimization and siRNAs was effective in increasing the MAGE-A4–specific TCR expression. PBMCs were transduced with the C-optiTCR retroviral vector and transfected with siRNA-a04 and siRNA-b03 (siRNA mixture) by electroporation. Introduction of the siRNA mixture reduced the endogenous TCR α and β RNA expression to 54% and 39% of the negative control siRNA-transferred PBMCs, respectively. The siRNA mixture did not affect the expression of the introduced codon-optimized TCR α or β chains (Fig. 2*C*). Tetramer staining

of MAGE-A4–specific TCRs showed that the siRNA mixture increased the cell surface MAGE-A4–specific TCR expression to levels ~1.6-fold greater than those observed with the control siRNA (Fig. 2*D*). These data indicate that the siRNA mixture specifically knocked down endogenous TCR RNA expression without inhibiting the introduced codon-optimized TCR, resulting in increased cell surface expression of the ectopic TCR.

Development of retroviral vectors that effectively express codon-optimized TCR and siRNAs targeting endogenous TCRs. We aimed to introduce lymphocytes with codon-optimized TCR α/β chains and siRNA targeting endogenous TCR using a single retroviral vector. To determine the most effective retroviral design, we constructed a total of 29 retroviral vectors and named them siTCR vectors (Fig. 1*B* and *C*). We generated constructs expressing siRNAs via short hairpin RNA transcription driven by pol III promoters (Fig. 1*B*) and constructs expressing pri-miRNA structures based on human miRNA miR-17/miR-18 clustered on the human genome and transcribed as a single transcriptional unit (34–36). This system uses the host processing system to generate mature siRNAs (Fig. 1*C*). A two-step selection process was done (Supplementary Fig. S1), and we selected the SH03, SH07, SH16, SH18, PM07, and PM11 siTCR vectors for further analysis (Supplementary Figs. S2 and S3).

Stable and effective expression of the ectopic TCR in lymphocytes transduced with siTCR retroviral vectors. We transduced PBMCs with the selected siTCR retroviral vectors and compared the cell surface expression of the ectopic TCR by staining with a specific tetramer. Transduction with SH16 and PM11 resulted in the highest percentage of tetramer-positive cells and the greatest mean fluorescent intensity (MFI; Fig. 3*A* and *B*). To select the best construct, we isolated tetramer-positive T cells and compared the endogenous TCR α and β gene knockdown efficiencies of SH16 and PM11. SH16 reduced the expression of endogenous TCR α and β to 10% and 60%, respectively, of the level observed in C-optiTCR–transduced T cells. On the other hand, PM11 reduced the expression of both endogenous TCR α and β to ~20% of the expression levels seen in C-optiTCR–transduced T cells (Fig. 3*C*). These results suggest that the siTCR vector PM11 is the most effective. To confirm the long-term expression of the introduced TCRs and the inhibition of endogenous TCRs, MAGE-A4$_{143\text{-}151}$ tetramer-positive T cells were separated from PM11 siTCR- and C-optiTCR–transduced PBMCs and cultured with interleukin-2 for 34 days after transduction. The proviral copy number, percentage of tetramer-positive cells, and TCR RNA expression levels were analyzed 4 and 34 days after transduction (Fig. 3*D*). In the PM11-transduced cells, all factors tested were sustained through day 34. Although the proviral copy number was slightly decreased at day 34, the percentage of tetramer-positive cells per proviral copy number was sustained through day 34. This shows that our siTCR constructs are able to maintain increased ectopic TCR expression and endogenous TCR α/β inhibition for >1 month.

Superiority of siTCR vectors in the expression of ectopic TCR with limited proviral copy number. We constructed an

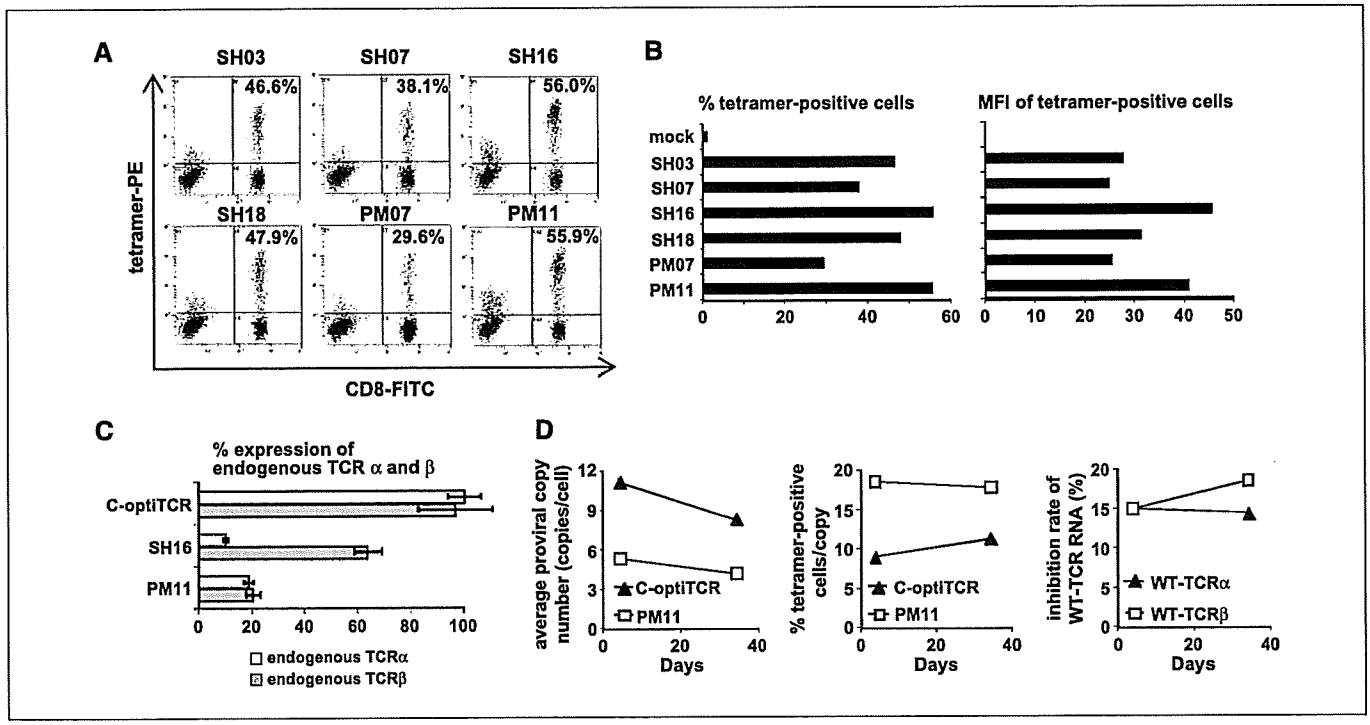

Figure 3. Efficient and stable expression of ectopic TCR using siTCR retroviral vectors. Activated PBMCs were transduced with the same volume of nondiluted indicated retroviral vectors or the control C-optiTCR retroviral vector. *A* and *B*, MAGE-A4 tetramer and anti-CD8 mAb staining. The numerical value indicates the percentage of tetramer-positive cells among CD8$^+$ cells (*A*). Percentage of tetramer-positive cells among CD8$^+$ cells (*B, left*) and MFI (*B, right*). These experiments were done using three donors' PBMCs with similar results. *C*, tetramer-positive cells were isolated and endogenous TCR α/β RNA expression was quantified. The expression level was calculated as the percentage of tetramer-positive cells isolated from C-optiTCR–transduced T cells. Representative of three independent experiments. These experiments were done using three donors' PBMCs with similar results. *D*, activated PBMCs were transduced with the PM11 or the C-optiTCR retroviral vector, and tetramer-positive cells were collected and cultured. The proviral copy number per cell (*left*) and the percentage of tetramer-positive cells per proviral copy number (*middle*) on days 4 and 34 were measured. Inhibition ratio per proviral copy number was calculated as (100 - RNA expression level) / proviral copy number (*right*). Representative of three independent experiments.

additional siTCR retroviral vector, PM11-w (Fig. 1*C*). Whereas the PM11 siTCR retroviral vector has one pair of siRNAs targeting WT-TCR α and β (siRNA-a04 and siRNA-b03), the PM11-w siTCR retroviral vector has an additional pair (siRNA-a06 and siRNA-b02), the inhibitory effects of which against WT-TCR α and β were equivalent to those of siRNA-a04 and siRNA-b03, respectively (data not shown). PBMCs were transduced with serially diluted C-optiTCR, PM11 siTCR, and PM11-w siTCR retroviral vectors. Following transduction, the average proviral copy number was evaluated, and MAGE-A4 tetramer staining and quantification of TCR RNAs were done. We plotted the percentage of tetramer-positive cells and the MFI of the tetramer-positive cells against the average copy number (Fig. 4*A, left* and *middle*). PM11 and PM11-w siTCR-transduced PBMCs showed greater number of tetramer-positive cells and a higher MFI compared with the C-optiTCR–transduced PBMCs. Importantly, for the C-optiTCR–transduced cells, twice the average copy number was needed to obtain the same rate of tetramer positivity compared with the siTCR-transduced cells. Similarly, five times the average copy number was required for C-optiTCR to achieve the same MFI level of tetramer staining when compared with the siTCR. The inhibition of RNA expression was highly correlated with the average copy number, and despite the use of bulk-transduced PBMCs that contained nontransduced cells, we could effectively reduce endogenous WT-TCR α/β expression levels (Fig. 4*A, right*). PM11-w–transduced PBMCs expressed a similar level of endogenous TCR α/β RNA when compared with PM11-transduced PBMCs.

To confirm the reproducibility of the effects of the siTCR retroviral vectors, PBMCs were transduced with serially diluted (1×, 2×, 4×, and 8×), conventional WT-TCR–expressing MS-bPa, C-optiTCR, PM11 siTCR, and PM11-w siTCR retroviral vectors and stained with MAGE-A4 tetramer. A comparable proviral copy number (3.1, 2.0, 2.4, and 2.7 copies per cell for MS-bPa–, C-optiTCR–, PM11-, and PM11-w–transduced T cells, respectively) was achieved with each vector at 8-, 4-, 1-, and 2-fold dilutions, respectively. As reported previously (15, 33), codon optimization (C-optiTCR) increased the surface expression of the TCR by ~1.85-fold compared with conventional WT-TCR (MS-bPa) gene transfer. Furthermore, the siTCR vectors (PM11 and PM11-w) induced MAGE-A4–specific TCR surface expression that was twice as high as that with codon optimization (with similar proviral copy number integration). In PM11-w–transduced T cells, the proportion of tetramer-positive cells was 4.6 times higher than in conventional MS-bPa–transduced cells and 2.5 times higher than in C-optiTCR–transduced cells. PM11-w–transduced T cells also had MFIs that were ~2.5 and 1.5 times higher than those of MS-bPa– and C-optiTCR–transduced cells, respectively (Fig. 4*B*).

To evaluate endogenous TCR α and β knockdown efficiencies, endogenous and exogenous MAGE-A4–specific TCR RNA expression levels were quantified in MAGE-$A4_{143\text{-}151}$ tetramer-positive T cells isolated from C-optiTCR–, PM11-, and PM11-w–transduced PBMCs with the comparable proviral copy numbers mentioned above. The endogenous TCR α and β expression levels in PM11 and PM11-w gene-modified T cells were reduced to 30% to 35% of the levels in C-optiTCR–transduced T cells, respectively. Although there was little difference in the inhibitory effects of endogenous TCR (Fig. 4*C, left*), the introduced TCR α and β RNA expression level was markedly higher in PM11-w–transduced cells compared with PM11-transduced cells (Fig. 4*C, right*). As stem-loop structures in the untranslated regions have been reported to inhibit polyadenylation and protect mRNA from degradation (37–39), it is suggested that the additional short hairpin RNA stem-loops in the PM11-w siTCR vector may act to stabilize the ectopic TCR RNA to achieve the high RNA expression level of the transduced TCR (Fig. 4*C, right*), thereby inducing strong expression of the introduced MAGE-A4–specific TCR α/β heterodimers on the T-cell surface.

Knockdown of endogenous TCRs at the protein level with facilitated expression of ectopic TCR heterodimers on the cell surface. We evaluated endogenous TCR expression in TCR gene-transferred cells at the cell surface protein level. Using PM11-w– and C-optiTCR–transduced PBMCs with comparable proviral copy numbers, we stained transduced cells with PE-labeled MAGE-$A4_{143\text{-}151}$/HLA-A*2402 tetramer and the mixture of FITC-labeled TCR Vβ antibodies (mixture of anti-Vβ2, Vβ3, and Vβ17 mAbs), none of which reacts with MAGE-A4–specific TCR. As shown in Fig. 4*D* (*left*), we found that staining with the mixture of anti-Vβ mAbs was markedly reduced in tetramer-positive cells compared with the tetramer-negative cells in both PM11-w– and C-optiTCR–transduced cells. Specifically, the MFIs for FITC in TCR Vβ antibody-positive cells in the tetramer-positive cells were reduced compared with those in the tetramer-negative cells (2,595 versus 6,715 in PM11-w–transduced cells and 3,219 versus 5,519 in C-optiTCR–transduced cells for PBMCs from donor 1; 2,902 versus 7,382 in PM11-w–transduced cells and 3,600 versus 7,027 for C-optiTCR–transduced cells from donor 2). Moreover, the MFIs for FITC in TCR Vβ antibody-positive cells in tetramer-positive cells were lower in PM11-w–transduced cells than in C-optiTCR–transduced cells for both donors. These results strongly suggest that TCR gene-modified T cells became tetramer-positive only when the cell surface expression of endogenous TCR was suppressed as a consequence of the competition for CD3 molecules between MAGE-A4–specific TCR α/β heterodimers and endogenous TCRs. We also performed single staining with a mixture of FITC-labeled TCR Vβ antibodies (Vβ2, Vβ3, and Vβ17) using PM11-w– and C-optiTCR–transduced PBMCs with comparable proviral copy numbers and mock-transduced PBMCs. As shown in Fig. 4*D* (*right*), the percentage of TCR Vβ-positive cells was reduced in TCR-transduced PBMCs with both constructs compared with mock-transduced PBMCs. Moreover, PM11-w–transduced PBMCs showed lower percentages of TCR Vβ-positive cells than C-optiTCR–transduced PBMCs.

Taken together with the finding that PM11-w–transduced cells showed a markedly increased number of tetramer-positive cells compared with C-optiTCR (Fig. 4*A* and *B*), these data suggest that the suppression of endogenous TCR by our siTCR retroviral vector facilitated increased expression of exogenous TCRs and yielded a larger population of MAGE-A4 tetramer-positive cells.

Enhanced antitumor cytotoxicity of lymphocytes transduced with the siTCR retroviral vector. We compared the function of T cells transduced with the C-optiTCR and PM11-w siTCR vector at similar proviral copy numbers. PBMCs were transduced with these retroviral vectors at several dilutions. Transduced T cells with comparable proviral copy numbers were selected for the CTL assay. In C-optiTCR– and PM11-w–transduced cells, the proviral copy numbers were 4.2 and 4.0 copies per cell, respectively, in the specific experiment shown in Fig. 5.

The lytic activity against the tumor cell line 11-18 (MAGE-$A4^+$/HLA-$A*2402^+$) differed between the two constructs: PM11-w–transduced PBMCs had greater lytic activity than C-optiTCR–transduced T cells. However, neither of the transduced cells showed lytic activity against the tumor cell line QG56, which

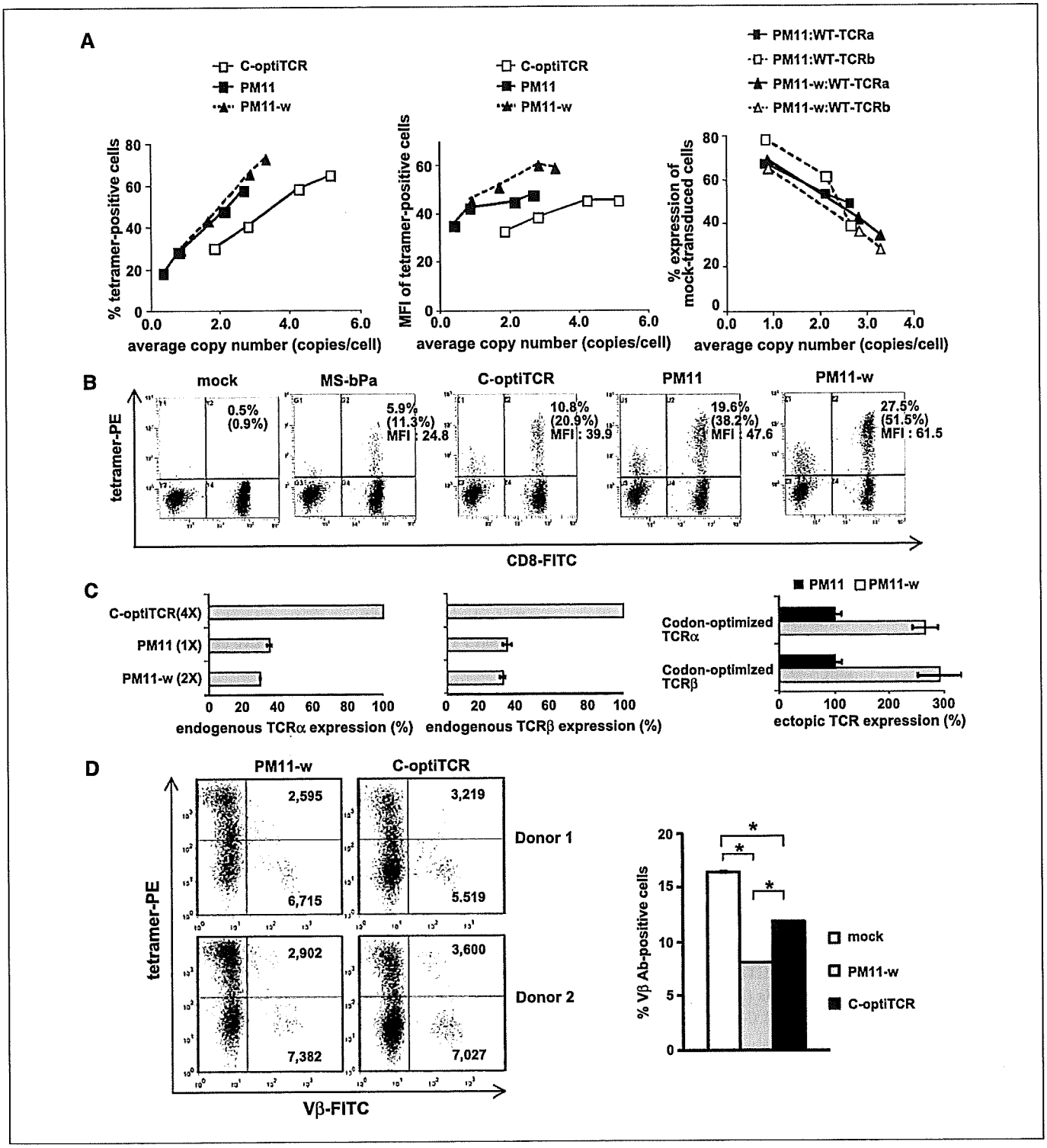

Figure 4. Superiority of siTCR vectors in the expression of an ectopic TCR and the suppression of endogenous TCRs with limited copy number. *A*, PBMCs were transduced with serially diluted PM11, PM11-w, or C-optiTCR retroviruses and used for proviral copy number analysis, tetramer staining, and quantification of endogenous TCR expression. Percentage of tetramer-positive cells among $CD8^+$ cells (*left*), MFIs (*middle*), and RNA expression level as the percentage of mock-transduced cells (*right*) are plotted according to copy number. *B*, representative flow cytometric analysis of PBMCs that were transduced with PM11, PM11-w, MS-bPa, or C-optiTCR retroviruses with equivalent proviral copy number. The numerical value indicates the percentage of tetramer-positive cells in whole cells, the percentage among $CD8^+$ cells (in parentheses), and MFI of tetramer-CD8 double-positive cells. *C*, tetramer-positive cells were collected. *Left*, endogenous TCR α and β mRNAs shown as the percentage of C-optiTCR(4×)–transduced PBMCs; *right*, RNA expression of ectopic TCR α/β in PM11(1×)- and PM11-w(2×)–transduced PBMCs was calculated as the percentage of PM11(1×)-transduced PBMCs. Representative of three independent experiments with PBMCs from two donors. *D*, activated PBMCs were transduced with PM11-w or C-optiTCR retroviruses. PBMCs with equivalent proviral copy numbers (donor 1: 3.4 copies per cell for PM11-w and 3.1 copies per cell for C-optiTCR; donor 2: 2.7 copies per cell for PM11-w and 2.5 copies per cell for C-optiTCR) were used for staining with tetramer and TCR Vβ mAb mixture (*left*) or for TCR Vβ mAb mixture single staining (*right*). The numerical value indicates the MFI for FITC in TCR Vβ-positive cells among tetramer-positive or tetramer-negative cells (*left*). Representative of three independent experiments. *, $P < 0.05$.

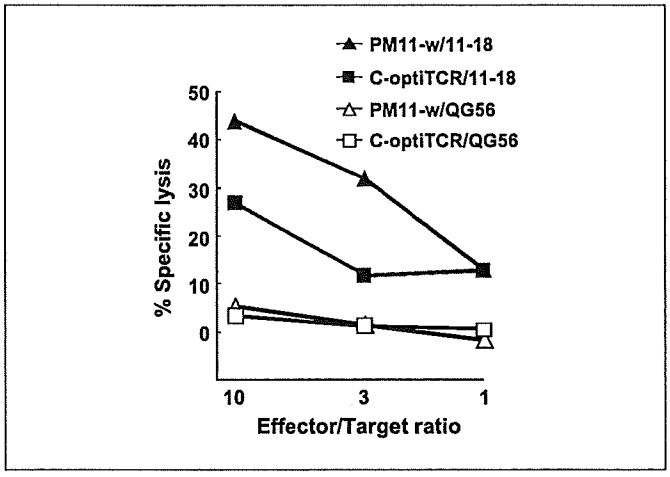

Figure 5. Enhanced tumor-specific CTL activity of gene-modified lymphocytes transduced with the siTCR retroviral vector. Activated PBMCs were transduced with serially diluted C-optiTCR or PM11-w siTCR retroviral vectors. PBMCs with equivalent proviral copy numbers were used for the cytotoxicity assay against 11-18 (MAGE-A4$^+$/HLA-A*2402$^+$) or QG56 (MAGE-A4$^+$/HLA-A*2402$^-$) cell lines.

lacks the restriction MHC (MAGE-A4$^+$/HLA-A*2402$^-$; Fig. 5). These results indicate that the higher expression of MAGE-A4–specific TCR in cells transduced with PM11-w-siTCR resulted in increased cytotoxic function of these cells.

Effectiveness of the siTCR retroviral vector encoding WT1-specific TCRs. To confirm the effectiveness of the siTCR retroviral vector for other TCRs, PBMCs were transduced with retroviral expression vectors for TCR α/β genes specific for the tumor antigen WT1 at several dilution factors followed by staining with the $WT1_{235\text{-}243}$/HLA-A*2402 tetramer (Fig. 6*A*). The constructs of these retroviral vectors are shown in Fig. 1*D*. WT1-siTCR–transduced PBMCs showed a higher percentage of tetramer-positive cells and a higher MFI compared with the control WT1-WT– or WT1-CO–transduced PBMCs with limited proviral copy number integration, showing the effectiveness of the siTCR vector on WT1-specific TCR α/β. When the transduced T cells with similar proviral copy number integration were compared, the proportion of tetramer-positive cells was 2.8 times higher, and the MFIs of tetramer-positive cells were 1.7 times higher than that of conventional WT1-WT–transduced cells (Fig. 6*B*). These results indicate that the effectiveness of our siTCR vector is not specific for one TCR and that this approach is applicable for other TCRs.

Discussion

In the present study, we developed retroviral vectors to simultaneously express siRNAs to silence endogenous TCR gene expression and a codon-optimized (siRNA-resistant), tumor antigen-specific TCR. In transduced lymphocytes, these novel vectors efficiently expressed the introduced TCR, reduced the expression of the endogenous TCR, and enhanced the antigen-specific lysis of target cells at a relatively low proviral copy number. Therefore, this new approach to TCR gene therapy has potential clinical relevance for treating patients with malignancies or uncontrollable virus infections such as cytomegalovirus infection after bone marrow transplantation, and it may help to reach the threshold for clinical response via infusion of TCR-engineered T cells.

The TCR-constant region-specific siRNAs used in this study increased the cell surface expression of the codon-optimized MAGE-A4–specific TCR (Fig. 2*D*). Although the surface expression increased, codon-optimized MAGE-A4–specific TCR α and β mRNA expression did not change significantly when siRNAs were introduced (Fig. 2*C*). Therefore, we conclude that a decrease in TCR mispairing and reduced competition for CD3 molecules between endogenous and ectopic TCR mediated the increased cell surface expression of the ectopic TCR.

Several strategies have been reported to reduce TCR mispairing and enhance CD3 molecule association. The introduction of an additional cysteine residue, which promotes the formation of a second disulfide bond, facilitated the expression and pairing of an ectopic TCR in human lymphocytes (18, 19, 25). Alternatively, the replacement of human C_α and C_β domains with corresponding murine C domains has been reported to improve the binding of ectopic TCR α and β chains and enhance the stability of the TCR/CD3 complex in human T cells (17, 19). Importantly, both methods resulted in increased reactivity against antigen-expressing tumor cells. However, the effectiveness of these methods was dependent on the variable region sequence of the TCR (19). It has been suggested that the enhanced association of the ectopic TCR chains disrupts "weak" TCR α/β combinations; however, this effect is minimized with "strong" TCR combinations in which the variable region sequences play an important role in efficient αβ pairing (16, 19, 20, 26). Despite the diversity of the variable region, the constant region consists of only one C_α and two C_β sequences ($C_\beta1$ and $C_\beta2$). The simplicity of the constant regions allowed us to suppress diverse TCR α and β rearrangements with only two siRNAs directed against the C_α region and the consensus $C_\beta1/C_\beta2$ sequence. Because the siRNAs used in this study were directed against the endogenous TCR constant regions, we believe that the effectiveness of the approach presented here can be universal for all TCR rearrangements, independent of the ectopic TCR V region sequence, as we showed the efficacy of the siTCR retroviral vector with WT1-specific TCR α/β (Fig. 6).

Several groups have shown the feasibility of retroviral TCR gene transfer to produce antigen-specific T cells for adoptive immunotherapy, and high retroviral transduction efficiency in T cells has been reported using the recombinant fibronectin fragment CH-296 (RetroNectin; refs. 1, 4–6, 40–44). However, the use of retroviral vectors in gene therapy has raised safety concerns because of nonspecific insertion into the human genome (7, 45–47). Although no side effects related to insertional mutagenesis have been reported in clinical settings following the retroviral transduction of mature T cells instead of CD34$^+$ bone marrow cells (48), continued follow-up will be required to assess the overall risk. Minimizing the viral vector copy number is preferable for any gene therapy approach even with mature cells (22, 24). Given this concern, our strategy is suitable for gene therapy as it can efficiently express an ectopic TCR with low proviral copy integration.

At a similar proviral copy number, transduction with PM11 and PM11-w resulted in 3.4- and 4.6-fold more tetramer-positive cells than the conventional WT-TCR vector and 1.8- and 2.5-fold more than the codon-optimized TCR vector, respectively. In addition, an average copy number of 4.86, 1.02, 0.60, and 0.58 copies per cell was required for the conventional WT-TCR vector, the codon-optimized TCR vector, the PM11 siTCR vector, and the PM11-w siTCR vector, respectively, to produce a similar percentage of tetramer-positive cells (16.0%, 14.5%, 13.6%, and 15.9%,

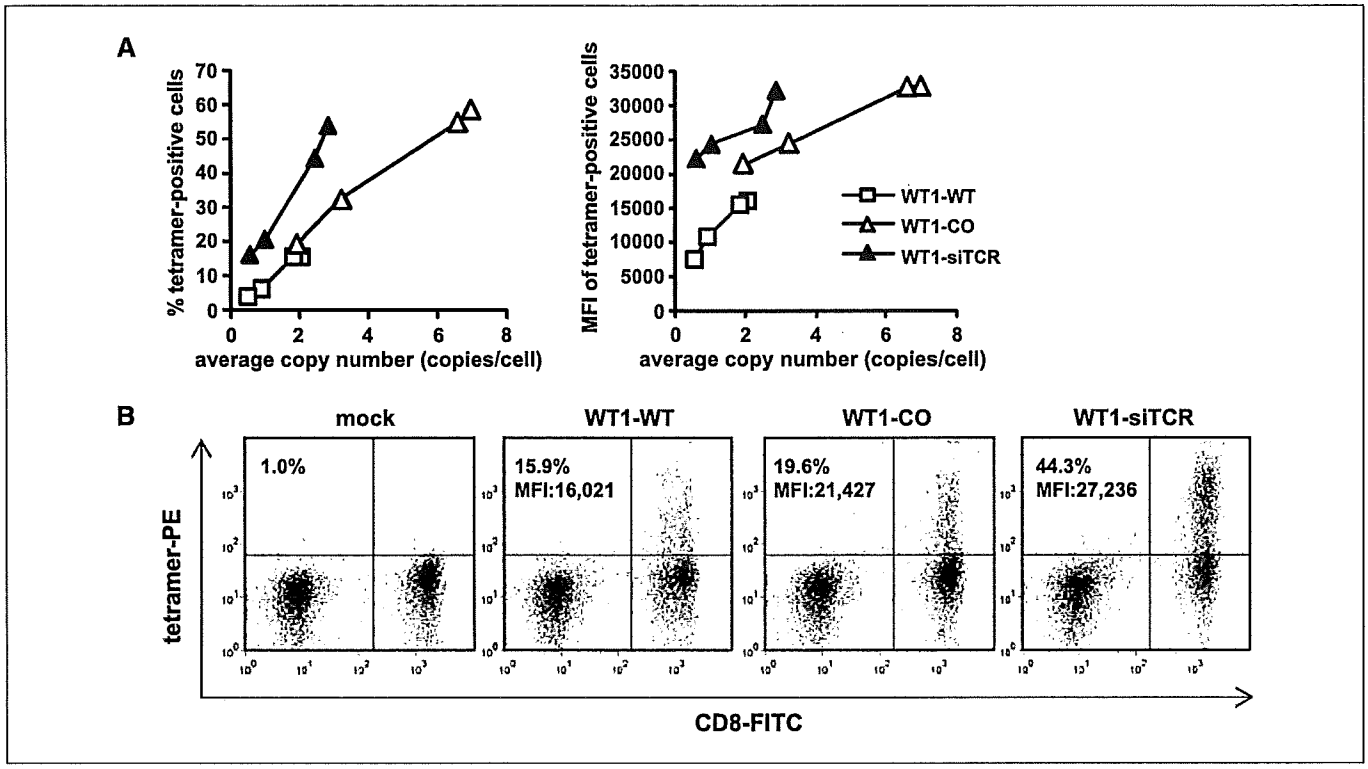

Figure 6. Effective expression of WT1-specific TCR α/β with siTCR retroviral vector. *A*, PBMCs were transduced with serially diluted WT1-WT, WT1-CO, or WT1-siTCR retroviruses and used for proviral copy number analysis and tetramer staining. Percentage of WT1 tetramer-positive cells among $CD8^+$ cells (*left*) and MFIs (*right*) are plotted according to copy number. Representative experiment of two donors' PBMCs. *B*, representative flow cytometric analysis with equivalent proviral copy number (2.1 for WT1-WT, 2.0 for WT1-CO, and 2.5 for WT1-siTCR). The numerical value indicates the percentage and MFI of tetramer-positive cells among $CD8^+$ cells. Representative experiment of two donors' PBMCs.

respectively; Fig. 4*B*; data not shown). These results were reflected in the biological function of the siTCR vector-transduced PBMCs: PM11-w–transduced cells showed greater cytotoxicity against antigen-expressing tumor cells than cell transduced with codon-optimized TCR vectors without siRNA (Fig. 5). To our knowledge, this study is the first to determine the efficiency of ectopic TCR expression based on the proviral copy number in the transduced cells. Our results clearly show the importance of this type of analysis for precise evaluation of the usefulness as well as the safety of each retroviral vector.

With regard to the clinical application of TCR gene therapy, cotransduction of several retroviral vectors may be challenging due to safety requirements, the cost of vector production and approval, and complications in their use, including the adjustment of retroviral vector titers. To overcome these problems, we aimed to develop constructs expressing multiple cassettes including a tumor antigen-specific TCR and two siRNAs targeting the endogenous TCR α/β. We tested these constructs using a short hairpin RNA cassette driven by a pol III promoter, which is one of the most generally used methods for expressing siRNAs (49, 50). As an alternative approach, we generated an expression cassette in which the siRNAs were expressed similarly to miRNAs. miRNAs are noncoding RNAs that regulate a variety of biological processes through complementary binding to target mRNAs, resulting in the direct inhibition of mRNA translation and/or destabilization of the target mRNA. miRNAs are expressed as long transcripts (pri-miRNAs) that are processed into ~70-nucleotide stem-loop forms (pre-miRNAs). The pre-miRNAs are finally cleaved in the cytoplasm by Dicer to generate mature miRNAs (34–36). After screening of a variety of vector constructs (Fig. 3; Supplementary Figs. S2 and S3), we found that the PM11 vector that used a cluster of pri-miRNAs was the most effective vector for ectopic expression of the TCR in T cells (Fig. 3). This vector was further modified to produce PM11-w, which carried two pairs of siRNAs against each TCR α and β. We found that this vector more efficiently expressed the TCR on the cell surface with a low proviral copy number compared with PM11 (Fig. 4*A* and *B*). Comparing the cells transduced with PM11 and PM11-w, we observed a similar inhibitory effect on endogenous TCR but higher expression of ectopic TCR mRNA in cells transduced with PM11-w (Fig. 4*C*). These data suggested that the RNA stabilization effect mediated the superiority of PM11-w to PM11 (37–39). Although the off-target effects of siRNAs need to be examined in detail before this method can be applied clinically, these data suggest that retroviral constructs such as PM11-w may prove useful for TCR gene therapy in cancer patients.

In summary, we showed a novel approach to TCR gene therapy that satisfies the following requirements: enhancement of ectopic TCR heterodimer cell surface expression and enhanced biological function at low proviral copy number (which may reduce the risk of mutagenesis); reduction of endogenous TCR expression, which may effectively reduce TCR mispairing and decrease the risk of inducing self-reactive TCR α/β heterodimers; and a universal method that does not depend on TCR variation. Such a novel approach to TCR gene therapy using siTCR retroviral vectors may prove useful for the development of effective and safe TCR gene therapy

protocols for patients with malignancies as well as those with viral infections.

Disclosure of Potential Conflicts of Interest

No potential conflicts of interest were disclosed.

Acknowledgments

Received 4/18/09; revised 9/17/09; accepted 9/24/09; published OnlineFirst 11/10/09.

The costs of publication of this article were defrayed in part by the payment of page charges. This article must therefore be hereby marked *advertisement* in accordance with 18 U.S.C. Section 1734 solely to indicate this fact.

We thank Dr. Masanari Kitagawa for designing the siRNAs, Emi Chatani and Risa Sumioka for expert technical contributions and suggestions, and Dr. Kiyotaka Kuzushima for generously providing $WT1_{235\text{-}243}$/HLA-A*2402 tetramer.

References

1. Morgan RA, Dudley ME, Yu YY, et al. High efficiency TCR gene transfer into primary human lymphocytes affords avid recognition of melanoma tumor antigen glycoprotein 100 and does not alter the recognition of autologous melanoma antigens. J Immunol 2003;171:3287–95.
2. Rubinstein MP, Kadima AN, Salem ML, et al. Transfer of TCR genes into mature T cells is accompanied by the maintenance of parental T cell avidity. J Immunol 2003;170:1209–17.
3. Zhao Y, Zheng Z, Robbins PF, Khong HT, Rosenberg SA, Morgan RA. Primary human lymphocytes transduced with NY-ESO-1 antigen-specific TCR genes recognize and kill diverse human tumor cell lines. J Immunol 2005;174:4415–23.
4. Hughes MS, Yu YY, Dudley ME, et al. Transfer of a TCR gene derived from a patient with a marked antitumor response conveys highly active T-cell effector functions. Hum Gene Ther 2005;16:457–72.
5. Coccoris M, Swart E, de Witte MA, et al. Long-term functionality of TCR-transduced T cells *in vivo*. J Immunol 2008;180:6536–43.
6. Abad JD, Wrzensinski C, Overwijk W, et al. T-cell receptor gene therapy of established tumors in a murine melanoma model. J Immunother 2008;31:1–6.
7. Sadelain M, Riviere I, Brentjens R. Targeting tumours with genetically enhanced T lymphocytes. Nat Rev Cancer 2003;3:35–45.
8. Murphy A, Westwood JA, Teng MW, Moeller M, Darcy PK, Kershaw MH. Gene modification strategies to induce tumor immunity. Immunity 2005;22:403–14.
9. June CH. Adoptive T cell therapy for cancer in the clinic. J Clin Invest 2007;117:1466–76.
10. Rosenberg SA, Restifo NP, Yang JC, Morgan RA, Dudley ME. Adoptive cell transfer: a clinical path to effective cancer immunotherapy. Nat Rev Cancer 2008;8:299–308.
11. Morgan RA, Dudley ME, Wunderlich JR, et al. Cancer regression in patients after transfer of genetically engineered lymphocytes. Science 2006;314:126–9.
12. Johnson LA, Morgan RA, Dudley ME, et al. Gene therapy with human and mouse T cell receptors mediates cancer regression and targets normal tissues expressing cognate antigen. Blood 2009;114:535–46.
13. Viola A, Lanzavecchia A. T cell activation determined by T cell receptor number and tunable thresholds. Science 1996;273:104–6.
14. Debets R, Willemsen R, Bolhuis R. Adoptive transfer of T-cell immunity: gene transfer with MHC-restricted receptors. Trends Immunol 2002;23:435–6.
15. Jorritsma A, Gomez-Eerland R, Dokter M, et al. Selecting highly affine and well-expressed TCRs for gene therapy of melanoma. Blood 2007;110:3564–72.
16. Stauss HJ, Cesco-Gaspere M, Thomas S, et al. Monoclonal T-cell receptors: new reagents for cancer therapy. Mol Ther 2007;15:1744–50.
17. Cohen CJ, Zhao Y, Zheng Z, Rosenberg SA, Morgan RA. Enhanced antitumor activity of murine-human hybrid T-cell receptor (TCR) in human lymphocytes is associated with improved pairing and TCR/CD3 stability. Cancer Res 2006;66:8878–86.
18. Cohen CJ, Li YF, El-Gamil M, Robbins PF, Rosenberg SA, Morgan RA. Enhanced antitumor activity of T cells engineered to express T-cell receptors with a second disulfide bond. Cancer Res 2007;67:3898–903.
19. Thomas S, Xue SA, Cesco-Gaspere M, et al. Targeting the Wilms tumor antigen 1 by TCR gene transfer: TCR variants improve tetramer binding but not the function of gene modified human T cells. J Immunol 2007;179:5803–10.
20. Sommermeyer D, Neudorfer J, Weinhold M, et al. Designer T cells by T cell receptor replacement. Eur J Immunol 2006;36:3052–9.
21. Heemskerk MH, Hagedoorn RS, van der Hoorn MA, et al. Efficiency of T-cell receptor expression in dual-specific T cells is controlled by the intrinsic qualities of the TCR chains within the TCR-CD3 complex. Blood 2007;109:235–43.
22. Kustikova OS, Wahlers A, Kuhlcke K, et al. Dose finding with retroviral vectors: correlation of retroviral vector copy numbers in single cells with gene transfer efficiency in a cell population. Blood 2003;102:3934–7.
23. Sadelain M. Insertional oncogenesis in gene therapy: how much of a risk? Gene Ther 2004;11:569–73.
24. Dropulic B. Genetic modification of hematopoietic cells using retroviral and lentiviral vectors: safety considerations for vector design and delivery into target cells. Curr Hematol Rep 2005;4:300–4.
25. Kuball J, Dossett ML, Wolfl M, et al. Facilitating matched pairing and expression of TCR chains introduced into human T cells. Blood 2007;109:2331–8.
26. Miyahara Y, Naota H, Wang L, et al. Determination of cellularly processed HLA-A2402-restricted novel CTL epitopes derived from two cancer germ line genes, MAGE-A4 and SAGE. Clin Cancer Res 2005;11:5581–9.
27. Hiasa A, Hirayama M, Nishikawa H, et al. Long-term phenotypic, functional and genetic stability of cancer-specific T-cell receptor (TCR) αβ genes transduced to $CD8^+$ T cells. Gene Ther 2008;15:695–9.
28. Nukaya I, Yasumoto M, Iwasaki T, et al. Identification of HLA-A24 epitope peptides of carcinoembryonic antigen which induce tumor-reactive cytotoxic T lymphocyte. Int J Cancer 1999;80:92–7.
29. Ohminami H, Yasukawa M, Fujita S. HLA class I-restricted lysis of leukemia cells by a CD8(+) cytotoxic T-lymphocyte clone specific for WT1 peptide. Blood 2000;95:286–93.
30. Makita M, Hiraki A, Azuma T, et al. Antilung cancer effect of WT1-specific cytotoxic T lymphocytes. Clin Cancer Res 2002;8:2626–31.
31. Tsuji T, Yasukawa M, Matsuzaki J, et al. Generation of tumor-specific, HLA class I-restricted human Th1 and Tc1 cells by cell engineering with tumor peptide-specific T-cell receptor genes. Blood 2005;106:470–6.
32. Neri S, Mariani E, Meneghetti A, Cattini L, Facchini A. Calcein-acetyoxymethyl cytotoxicity assay: standardization of a method allowing additional analyses on recovered effector cells and supernatants. Clin Diagn Lab Immunol 2001;8:1131–5.
33. Hart DP, Xue SA, Thomas S, et al. Retroviral transfer of a dominant TCR prevents surface expression of a large proportion of the endogenous TCR repertoire in human T cells. Gene Ther 2008;15:625–31.
34. Hayashita Y, Osada H, Tatematsu Y, et al. A polycistronic microRNA cluster, miR-17-92, is overexpressed in human lung cancers and enhances cell proliferation. Cancer Res 2005;65:9628–32.
35. Samols MA, Hu J, Skalsky RL, Renne R. Cloning and identification of a microRNA cluster within the latency-associated region of Kaposi's sarcoma-associated herpesvirus. J Virol 2005;79:9301–5.
36. Mineno J, Okamoto S, Ando T, et al. The expression profile of microRNAs in mouse embryos. Nucleic Acids Res 2006;34:1765–71.
37. Klasens BI, Das AT, Berkhout B. Inhibition of polyadenylation by stable RNA secondary structure. Nucleic Acids Res 1998;26:1870–6.
38. Suay L, Salvador ML, Abesha E, Klein U. Specific roles of 5′ RNA secondary structures in stabilizing transcripts in chloroplasts. Nucleic Acids Res 2005;33:4754–61.
39. Pavithra L, Rampalli S, Sinha S, Sreenath K, Pestell RG, Chattopadhyay S. Stabilization of SMAR1 mRNA by PGA2 involves a stem loop structure in the 5′ UTR. Nucleic Acids Res 2007;35:6004–16.
40. Kimizuka F, Taguchi Y, Ohdate Y, et al. Production and characterization of functional domains of human fibronectin expressed in *Escherichia coli*. J Biochem 1991;110:284–91.
41. Hanenberg H, Xiao XL, Dilloo D, Hashino K, Kato I, Williams DA. Colocalization of retrovirus and target cells on specific fibronectin fragments increases genetic transduction of mammalian cells. Nat Med 1996;2:876–82.
42. Chono H, Yoshioka H, Ueno M, Kato I. Removal of inhibitory substances with recombinant fibronectin-CH-296 plates enhances the retroviral transduction efficiency of CD34(+)CD38(−) bone marrow cells. J Biochem 2001;130:331–4.
43. Lamers CH, Willemsen RA, Luider BA, Debets R, Bolhuis RL. Protocol for gene transduction and expansion of human T lymphocytes for clinical immunogene therapy of cancer. Cancer Gene Ther 2002;9:613–23.
44. Quintas-Cardama A, Yeh RK, Hollyman D, et al. Multifactorial optimization of γ retroviral gene transfer into human T lymphocytes for clinical application. Hum Gene Ther 2007;18:1253–60.
45. Baum C, Dullmann J, Li Z, et al. Side effects of retroviral gene transfer into hematopoietic stem cells. Blood 2003;101:2099–114.
46. Yi Y, Hahm SH, Lee KH. Retroviral gene therapy: safety issues and possible solutions. Curr Gene Ther 2005;5:25–35.
47. Hacein-Bey-Abina S, Von Kalle C, Schmidt M, et al. LMO2-associated clonal T cell proliferation in two patients after gene therapy for SCID-X1. Science 2003;302:415–9.
48. Recchia A, Bonini C, Magnani Z, et al. Retroviral vector integration deregulates gene expression but has no consequence on the biology and function of transplanted T cells. Proc Natl Acad Sci U S A 2006;103:1457–62.
49. Elbashir SM, Harborth J, Lendeckel W, Yalcin A, Weber K, Tuschl T. Duplexes of 21-nucleotide RNAs mediate RNA interference in cultured mammalian cells. Nature 2001;411:494–8.
50. Yu JY, DeRuiter SL, Turner DL. RNA interference by expression of short-interfering RNAs and hairpin RNAs in mammalian cells. Proc Natl Acad Sci U S A 2002;99:6047–52.

Int J Hematol (2009) 89:251–252
DOI 10.1007/s12185-008-0251-8

LETTER TO THE EDITOR

Growth deceleration in a girl treated with imatinib

Tomiko Kimoto · Masami Inoue · Keisei Kawa

Received: 19 November 2008 / Revised: 3 December 2008 / Accepted: 18 December 2008 / Published online: 20 January 2009

Imatinib is an inhibitor of tyrosine kinase as well as BCR-ABL, platelet-derived growth factor receptor (PDGF-R) and c-kit, and is becoming a first-line treatment for chronic myeloid leukemia (CML). In children, the long-term toxic effects related to the inhibition of tyrosine kinase are not yet well understood.

A 6-year-old girl was diagnosed with BCR-ABL positive CML in the chronic phase in June 2003. After receiving imatinib (400 mg/m^2 per day), molecular remission was achieved and persisted for 4 years without major side-effects. At the beginning of imatinib administration, the patient was aged 6 years, and her height was 114 cm (−0.7SD). Her growth rate decreased during these 4 years, and her height was 121 cm (−2.7SD) when she was aged 11 years.

The patient followed the normal growth pattern since birth she had normal body proportions and appearance, no family history of short stature. Following extensive tests, she reached the normal GH peak after two stimulatory tests and other systemic diseases (endocrine disorder, renal failure, inflammatory disorders) were excluded.

Additionally, we identified delayed bone age on X ray of her wrists at the age of 11 years (bone age was 7 years) and low bone mineral density was demonstrated on dual-energy X ray absorptiometry of the lumbar spine (0.576 g/m^2 Z score less than −2.5SD for chronological age).

Bone formation markers (serum osteocalcin, 8.5 ng/ml and bone specific alkaline phosphatase BAP, 30.0 U/L) were lower than those of age-matched healthy girls (reference range; osteocalcin 36–93 ng/ml, BAP 66–137 IU/l) and bone resorption marker (urinary deoxypyridinoline 5.8 nM/mMCre) was also lower (reference range 28–42 mM/mMCre), suggesting that effect of decreased bone formation exceeded that of decreased bone resorption.

Because she had not been exposed to a long-term immunosuppressive steroid treatment and there were no other risk factor of inhibition of bone formation, we strongly suspected that imatinib treatment may have been associated with the low mineral density in this patient. After confirming the absence of detectable BCR-ABL trasnscript, imatinib was discontinued in October 2007, which subsequently resulted in gradual growth acceleration.

However, because BCR-ABL transcript in her peripheral blood reappeared, she was prepared for allogeneic stem cell transplantation.

We noted increased bone formation markers (BAP 110.9 U/L, osteocalcin 22.9 ng/ml) 8 months after discontinuation of imatinib, as well as an increased growth rate (6.2 cm over 8 months) (Fig. 1).

The possibility that imatinib restrains bone resorption (by inhibiting c-Fms on osteoclasts) and stimulates bone formation (by inhibiting PDGF-R on osteoblats) has been reported in vitro [1–3], and adult CML patients actually have increased bone volume after long-term imatinib therapy [4].

Although bone metabolism in our patient differed from that in adults receiving imatinib, we suspect that growth deceleration and low bone mineral density in our patient were associated with imatinib administration.

In September 2008 (11 months after discontinuation of imatinib), the patient has successfully achieved complete donor chimerism from an unrelated cord blood donor following reduced intensity conditioning with the expectation that she would achieve puberty and accelerated growth.

T. Kimoto (✉) · M. Inoue · K. Kawa
Department of Hematology/Oncology,
Osaka Medical Center and Research Institute
for Maternal and Child Health, 840 Murodo-cho,
Izumi, Osaka 594-1101, Japan
e-mail: tomiko@mch.pref.osaka.jp

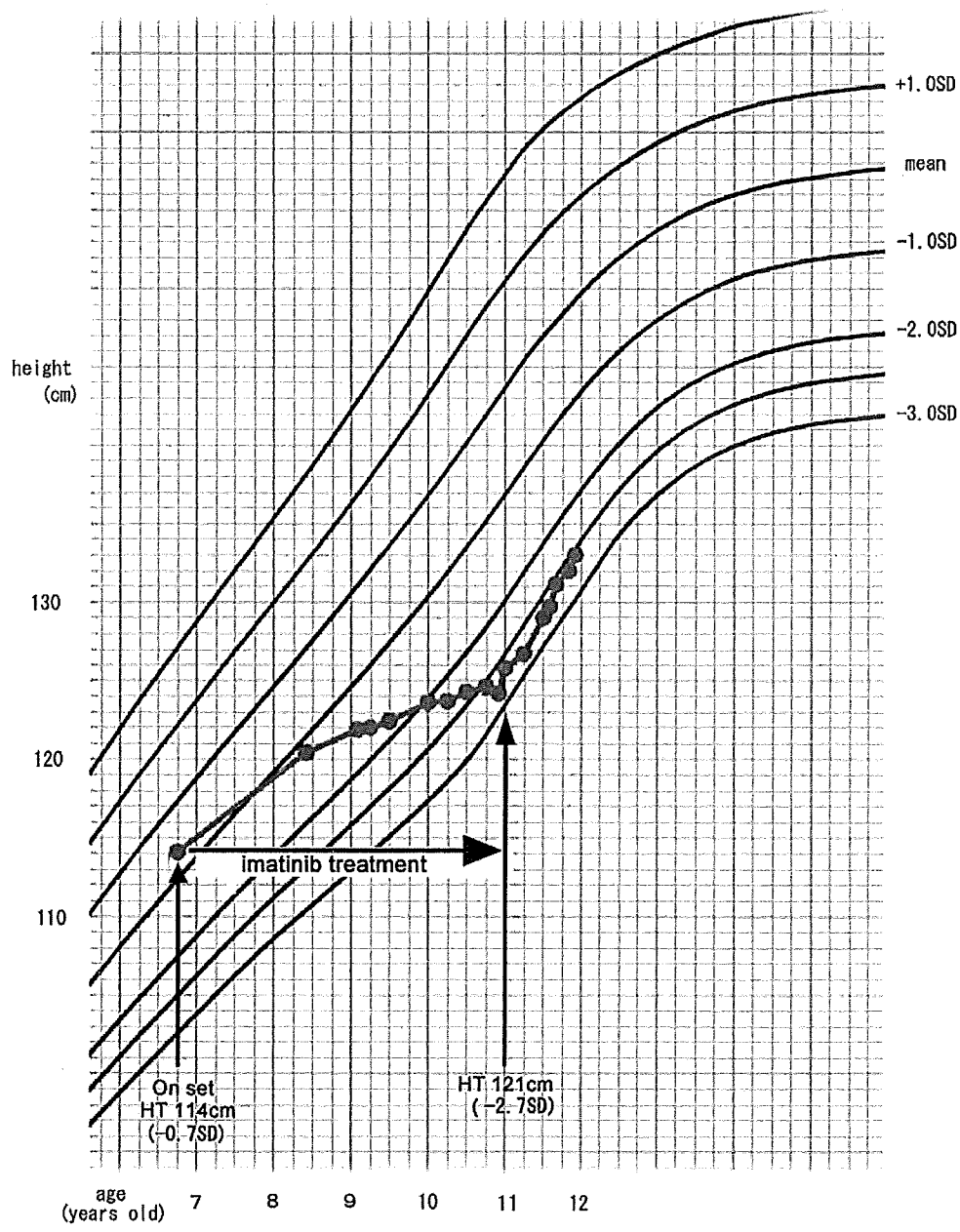

Fig. 1 Growth curve for height in the patient treated with imatinib compared to normal height curve, girls; growth deceleration during imatinib treatment and growth acceleration after discontinuation of it

Since our experience of long-term imatinib therapy during childhood is limited, further investigation is required to assess the late effects of this agent on growth.

References

1. Berman E, Nicolaides M, Maki RG, et al. Altered bone and mineral metabolism in patients receiving imatinib mesylate. N Engl J Med. 2006;354:2006–13. doi:10.1056/NEJMoa051140.
2. Grey A, O'Sullivan S, Reid IR, Browett P. Imatinib mesylate, increased bone formation, and secondary hyperparathyroidism. N Engl J Med. 2006;355:2494–5. doi:10.1056/NEJMc062388.
3. Dewar AL, Farrugia AN, Condina MR, et al. Imatinib as a potential antiresorptive therapy for bone disease. Blood. 2006;107:4334–7. doi:10.1182/blood-2005-09-3568.
4. Fitter S, Dewar AL, Kostakis P, et al. Long-term imatinib therapy promotes bone formation in CML patients. Blood. 2008;111:2538–47. doi:10.1182/blood-2007-07-104281.

Int J Hematol (2009) 90:492–500
DOI 10.1007/s12185-009-0402-6

ORIGINAL ARTICLE

A study of rasburicase for the management of hyperuricemia in pediatric patients with newly diagnosed hematologic malignancies at high risk for tumor lysis syndrome

Akira Kikuchi · Hisato Kigasawa · Masahito Tsurusawa · Keisei Kawa · Atsushi Kikuta · Masahiro Tsuchida · Yoshihisa Nagatoshi · Keiko Asami · Keizo Horibe · Atsushi Makimoto · Ichiro Tsukimoto

Received: 24 February 2009 / Revised: 20 July 2009 / Accepted: 27 July 2009 / Published online: 22 August 2009

Abstract Tumor lysis syndrome (TLS), including hyperuricemia, is a frequent serious complication in patients with hematologic malignancies. This study in Japanese patients evaluated the efficacy, safety, and pharmacokinetic profile of rasburicase in pediatric patients with hematologic malignancies. Patients aged <18 years at high risk for TLS, with newly diagnosed hematologic malignancies, were randomized to intravenous rasburicase 0.15 mg/kg/day ($n = 15$) or 0.20 mg/kg/day ($n = 15$) for 5 days. Chemotherapy was started 4–24 h after the first rasburicase dose. Response was defined as a reduction in plasma uric acid to ≤6.5 mg/dL (patients <13 years) or ≤7.5 mg/dL (patients ≥13 years) by 48 h after the first administration, lasting until 24 h after the final administration. Response rates were 93.3 and 100% with rasburicase 0.15 and 0.20 mg/kg/day, respectively. Uric acid levels declined rapidly within 4 h of starting rasburicase administration in both groups. Most adverse events were related to the underlying chemotherapy regimens. Two hypersensitivity reactions, including grade 1/2 pruritus, were considered to be related to rasburicase. Rasburicase is effective and well tolerated for the management of hyperuricemia in Japanese pediatric patients at high risk of developing TLS.

A. Kikuchi
Division of Hematology/Oncology,
Saitama Children's Medical Center, Saitama, Japan

A. Kikuchi (✉)
Department of Pediatrics, Graduate School of Medicine,
The University of Tokyo, 7-3-1 Hongo Bunkyo-ku,
Tokyo 113-8655, Japan
e-mail: akikuchi-tky@umin.ac.jp

H. Kigasawa
Department of Hemato-oncology/Regeneration Medicine,
Kanagawa Children's Medical Center, Yokohama, Japan

M. Tsurusawa
Department of Pediatrics, Aichi Medical University Hospital,
Aichi, Japan

K. Kawa
Department of Hematology/Oncology,
Osaka Medical Center and Research Institute for Maternal
and Child Health, Osaka, Japan

A. Kikuta
Department of Pediatrics, Fukushima Medical University
Hospital, Fukushima, Japan

M. Tsuchida
Department of Pediatrics, Ibaraki Children's Hospital,
Mito, Japan

Y. Nagatoshi
Department of Pediatrics, National Kyushu Cancer Center,
Fukuoka, Japan

K. Asami
Department of Pediatrics, Niigata Cancer Center Hospital,
Niigata, Japan

K. Horibe
Department of Pediatrics, National Hospital Organization,
Nagoya Medical Center, Nagoya, Japan

A. Makimoto
Department of Pediatrics, National Cancer Center Hospital,
Tokyo, Japan

I. Tsukimoto
Children's Center, Saiseikai Yokohamasi Tobu Hospital,
Yokohama, Japan

Keywords Hematologic malignancies · Hyperuricemia · Pediatric · Rasburicase · Tumor lysis syndrome (TLS)

1 Introduction

Patients with hematologic malignancies are usually treated with aggressive chemotherapy regimens that result in the rapid destruction of tumor cells and the release of purine metabolites into the circulation [1]. This may lead to the development of tumor lysis syndrome (TLS), which is characterized by severe hyperuricemia, hyperphosphatemia, hyperkalemia, and hypocalcemia [2, 3]. Moreover, as a consequence of hyperuricemia, crystals of uric acid may form in the renal tubules and distal collecting system, leading to renal insufficiency and acute renal failure [4]. Patients with malignancies that have a high proliferation rate or a large tumor burden, such as acute lymphoblastic leukemia or Burkitt's lymphoma, have a particularly high risk of developing TLS. The metabolic disturbances resulting from TLS may lead to acute renal failure and rapidly become life threatening in pediatric patients. Appropriate management for metabolic abnormalities in these patients is therefore essential in order to reduce the risk of developing acute renal failure [5–7].

The current treatment of hyperuricemia in Japan includes urinary alkalinization, hydration, and allopurinol. Allopurinol inhibits xanthine oxidase and thus prevents the formation of uric acid and controls plasma uric acid levels during purine catabolism [4]. Allopurinol, however, cannot reduce the level of pre-existing uric acid and causes increases in serum levels of xanthine and hypoxanthine, which may lead to xanthine nephropathy [8, 9]. In addition, urinary alkalinization can cause renal precipitation of calcium phosphate [4].

Rasburicase is a recombinant form of the endogenous enzyme urate oxidase. It is produced following the proteolytic hydrolysis of *Aspergillus flavus* urate oxidase, which permits the formation of oligodeoxynucleotide probes that are used to obtain DNA fragments from *Aspergillus flavus* cDNA and genomic libraries [10]. Rasburicase is approved for the prevention and treatment of hyperuricemia in children with leukemia or lymphoma in the USA and the EU. This agent oxidizes uric acid, converting it to allantoin, a substance that is approximately 5–10 times more soluble than uric acid and is easily excreted in the urine [8]. Rasburicase is administered intravenously, making it more convenient to administer to patients with chemotherapy-associated gastrointestinal toxicities than the oral drug allopurinol. Moreover, rasburicase can reduce pre-existing uric acid levels [11].

In a US open-label, randomized study in 52 children with leukemia or lymphoma at high risk for TLS, administration of rasburicase (0.20 mg/kg/day) for 5–7 days during induction chemotherapy achieved significantly more rapid control of uric acid and lower levels of plasma uric acid than allopurinol (300 mg/m^2/day) for 5–7 days [12]. This led the investigators to conclude that rasburicase is a safe and an effective alternative to allopurinol during initial chemotherapy in pediatric patients.

The aim of this study was to investigate the efficacy, safety, and pharmacokinetic profile of rasburicase as a single agent in Japanese pediatric patients with hematologic malignancies at high risk for TLS. In particular, the safety of rasburicase administered before chemotherapy was evaluated in this patient population.

2 Materials and methods

2.1 Study design and patients

This was a multicenter, open-label, randomized, parallel-group study of repeated doses of rasburicase in Japanese pediatric patients with newly diagnosed hematologic malignancies at high risk of developing TLS.

The study protocol was approved by the institutional review boards of all participating centers. Written informed consent was obtained from the legally authorized representative of each patient before randomization to one of two doses of rasburicase (0.15 or 0.20 mg/kg).

Japanese pediatric patients (aged <18 years) were eligible for study entry if they had newly diagnosed hematologic malignancies with hyperuricemia (uric acid >7.5 mg/dL for patients aged ≥13 years; uric acid >6.5 mg/dL for patients aged <13 years) or newly diagnosed hematologic malignancies presenting with a high tumor burden, regardless of uric acid level [defined as non-Hodgkin's lymphoma (NHL) stage IV; NHL stage III with at least one lymph node or mass >5 cm in diameter or lactate dehydrogenase (LDH) three or more times the upper limit of normal (ULN)]; or acute leukemia with a white blood cell (WBC) count ≥50,000/mm^3 and LDH three or more times ULN. Patients were required to have a performance status of 3 or less on the Eastern Cooperative Oncology Group (ECOG) scale (or 30 or more on the Lansky score) and a minimum life expectancy of 45 days. Patients received induction chemotherapy between 4 and 24 h after the first administration of rasburicase.

Exclusion criteria included the administration of allopurinol within 72 h before the start of rasburicase administration; known history of severe allergy and/or severe asthma; low birth weight (<2,500 g) or gestational age (<37 weeks); previous therapy with urate oxidase; known positive tests for hepatitis B surface antigen, hepatitis C virus antibodies, or HIV-1 or HIV-2 antibodies; severe

disorders of the liver or kidney [alanine aminotransferase (ALT) levels more than five times ULN, total bilirubin more than three times ULN, creatinine more than three times ULN]; or uncontrollable infection (including viral infection). The enzymatic conversion of uric acid to allantoin by rasburicase produces hydrogen peroxide [13]. This can lead to methemoglobinemia and hemolysis in certain "at-risk" populations such as those with glucose-6-phosphate dehydrogenase (G6PD) deficiency, and hence G6PD deficiency contraindicates the use of rasburicase. Therefore, patients with a known family history of G6PD deficiency, and known history of methemoglobinemia and hemolysis, were also excluded.

Randomization was performed centrally, and patients were stratified by baseline weight (<10 or ≥10 kg) until 15 patients had been enrolled in each dose group. To ensure the exact evaluation of pharmacokinetics, at least 10 patients weighing ≥10 kg were included in each dose group. The protocol did not require that a minimum number of patients weighing <10 kg should be enrolled.

2.2 Treatment

Rasburicase (SR29142) was supplied by sanofi-aventis (Tokyo, Japan). Patients were randomized to one of two dose groups of rasburicase (0.15 or 0.20 mg/kg). Rasburicase 0.20 mg/kg has been approved in 50 countries worldwide, but in the USA, the doses of rasburicase 0.15 and 0.20 mg/kg have been approved. Given that the efficacy of rasburicase 0.15 and 0.20 mg/kg was recently demonstrated in a previous study in adult Japanese patients [14], both these doses were selected for use in this pediatric trial. Rasburicase was administered intravenously for 30 min once daily for 5 consecutive days.

Chemotherapy, including cytoreductive corticosteroids, was started 4–24 h after the first dose of rasburicase. Separate lines were used for administration of chemotherapy and infusion of rasburicase to prevent drug–drug interactions. When this was not possible, the line was flushed with isotonic saline (≥15 mL) before and after infusion of rasburicase. Other anti-hyperuricemic agents (e.g. allopurinol) or treatment with sodium bicarbonate for urine alkalization were not permitted until the final blood sampling for plasma uric acid was completed on day 6.

2.3 Efficacy assessments

The primary efficacy endpoint was response rate (RR), as determined by assays of plasma uric acid concentration. Treatment was considered to be successful and the patient considered to be a responder if the plasma uric acid level decreased to ≤7.5 mg/dL in patients aged ≥13 years or ≤6.5 mg/dL in patients aged <13 years by 48 h after the start of the first rasburicase administration, and lasting until 24 h after the start of the final rasburicase administration (day 5).

Secondary endpoints included plasma uric acid concentration and change in concentration from baseline. The rate of plasma uric acid inhibition over time versus baseline was also evaluated at 4 and 48 h after the first rasburicase administration and at 24 h after the last rasburicase administration. The rate of uric acid inhibition (%) was calculated as the concentration of plasma uric acid at baseline minus the concentration of plasma uric acid at each timepoint divided by the concentration at baseline multiplied by 100. Blood samples were collected for the plasma uric acid levels ≤10 min before and 4 h (±10 min) after the first rasburicase administration on day 1; samples were also collected before rasburicase administration (±10 min) on days 2–5, and 24 h (±10 min) after the last rasburicase administration on day 6.

2.4 Safety assessments

Safety was assessed by clinical observations (including vital signs), standard laboratory tests, and the occurrence of adverse events (AEs). AEs were summarized by type of event and toxicity grade according to the National Cancer Institute Common Terminology Criteria for Adverse Events version 3.0 (translated into Japanese by the Japan Clinical Oncology Group/Japan Society of Clinical Oncology). These events were classified by each investigator as either rasburicase-related or other (related to underlying hematologic malignancies or chemotherapy). Rasburicase-related AEs were defined as all events excluding events due to the underlying disease or chemotherapy. Renal function (creatinine, potassium, phosphorus, and calcium levels) was also assessed at baseline (7 days before starting the first administration of rasburicase), and on day 3, 5, 8, 15, 22, 29, and 36.

2.5 Evaluation of anti-rasburicase antibodies

To evaluate the relationship between hypersensitivity reactions and the appearance of anti-rasburicase antibodies, the antibodies were assessed by qualitative enzyme-linked immunosorbent assay (ELISA) at baseline and on day 29. The results were expressed qualitatively due to the lack of immunopurified reference human antibody directed against rasburicase, with the conventional properties of antibodies utilized to detect antibodies directed against rasuburicase. The range of anti-human immunoglobulin calibration was between 0 and 1,000 ng/mL and plasma samples from healthy volunteers were used as reference controls. Plasma collected from healthy volunteers was assayed by ELISA

to determine background interference in the detection of anti-rasburicase immunoglobulin. If the samples were positive for anti-rasburicase antibodies on day 29, then further blood samples were collected from the patient at 6 months (±2 weeks) and every 6 months (±2 weeks) thereafter until the sample was negative. Samples that were antibody positive were analyzed for inhibition of rasburicase uricolytic activity. Anti-*S. cerevisiae* protein (SCP) antibodies were also assessed by ELISA at baseline.

2.6 Pharmacokinetics

The pharmacokinetic assay was performed in 10 patients (weight ≥10 kg) in each dose group at the following 10 timepoints: Day 1, before rasburicase administration (within 10 min of the start of administration), at the end of the first administration (within 10 min following completion of administration), 4 and 8 h (±10 min) after the start of administration; day 2, before rasburicase administration (within 10 min of the start of administration); and day 5, before rasburicase administration (within 10 min of the start of administration), at the end of administration, 4, 8, and 24 h (±10 min) after the last administration. A total sample of 10 mL from each patient was immediately centrifuged at <4°C and then frozen until assay. Frozen samples were sent to the laboratories (SBI-BIO, Paris, France), where they were assayed concomitantly.

The following pharmacokinetic parameters were determined: area under the rasburicase plasma concentration–time curve from 0 to 24 h (AUC_{0-24}) on days 1 and 5; minimum rasburicase plasma concentration observed before treatment administration during repeated dosing (C_{min}) on days 1 and 5; plasma concentration of rasburicase at the end of infusion (C_{eoi}) on days 1 and 5; terminal half-life ($t_{1/2z}$) on day 5; and accumulation ratio for AUC_{0-24} and C_{eoi} (defined as the ratio of day 5 to day 1 for AUC_{0-24} and C_{eoi}). Rasburicase plasma concentrations were determined by ELISA.

2.7 Statistical analysis

All patients who received at least one dose of rasburicase were evaluated for efficacy and safety. The RR, with 95% exact binomial confidence intervals (CIs), was calculated as the number of responding patients divided by the number of evaluable patients multiplied by 100. Patients who failed to complete days 1–5 of treatment, for reasons other than hyperuricemia, were considered as nonevaluable for RR. Descriptive statistics were used to summarize uric acid concentrations, and change from baseline and the rate of plasma uric acid concentration decline over time.

For the purposes of the statistical analysis, the study had a planned sample size of 30 patients, i.e. 15 in each dose group (0.15 and 0.20 mg/kg). Assuming that the true RR would be 95% in each dose group, the probability of at least one failure among 15 patients treated with each dose of rasburicase would be 79%, with an expected lower 95% CI of 71%. Based on a sample size of 15 patients per dose group, it could therefore be concluded with 95% confidence that the true RR would be at least 71%.

Pharmacokinetic parameters for rasburicase were determined using WinNonlin Professional Edition software (version 3.3 Pharsight Corp, Mountain View, CA, USA) using a noncompartmental method. To assess drug accumulation from day 1 to day 5, the parameters AUC_{0-24} and C_{eoi} were analyzed using the linear mixed-effects model:

$$\text{Log (parameter)} = \text{dose} + \text{day} + \text{dose} \times \text{day} + \text{patient (dose)} + \text{error}$$

Fixed-effect terms included dose (0.15 and 0.20 mg/kg), day (1 and 5), and the interaction term dose by day. The random-effect term was patient within dose. The model was estimated using generalized least squares (GLS) with restricted maximum likelihood (REML) estimates of random effects, using SAS® PROC MIXED.

The 95% CIs for the variance estimates were computed using the simple chi-squared method for within-patient variance, the Modified Large Sample procedure for between-patient variance, and the Graybill–Wang procedure for the total-patient variance [15].

3 Results

3.1 Patients

Between June 2005 and April 2006, 31 patients were enrolled and 30 patients were subsequently randomized and treated (rasburicase 0.15 mg/kg, $n = 15$; rasburicase 0.20 mg/kg, $n = 15$). One enrolled patient was not randomized to treatment because of an ineligible ALT level. This patient was excluded from the efficacy and safety analyses.

Patient baseline characteristics were similar between the rasburicase dose groups (Table 1). The median age was 8.8 years, and over half of the patients (53.3%) were aged between 6 and 12 years. Overall median weight was 30.8 kg, and one patient weighed <10 kg. Most patients had an ECOG performance status of 0 (40%) or 1 (40%). A total of 43.3% of patients were hyperuricemic, and 73.3% of patients had acute leukemia. All patients were classified as high risk for TLS in accordance with the inclusion criteria (i.e. had a newly diagnosed hematologic malignancy with hyperuricemia or a high tumor burden).

Table 1 Baseline characteristics of randomized patients

	Rasburicase		Total (n = 30)
	0.15 mg/kg (n = 15)	0.20 mg/kg (n = 15)	
Age (years)			
Median	11	7	9
Range	1–17	0–16	0–17
Age group, n (%)			
<2 years	1 (6.7)	1 (6.7)	2 (6.7)
2–5 years	2 (13.3)	4 (26.7)	6 (20.0)
6–12 years	7 (46.7)	9 (60.0)	16 (53.3)
13–17 years	5 (33.3)	1 (6.7)	6 (20.0)
Male/female, n (%)	9/6 (60.0/40.0)	10/5 (66.7/33.3)	19/11 (63.3/36.7)
Weight (kg)			
Median	44.7	25.5	30.8
Range	10.2–70.3	5.7–49.7	5.7–70.3
ECOG performance status, n (%)			
0	7 (46.7)	5 (33.3)	12 (40.0)
1	5 (33.3)	7 (46.7)	12 (40.0)
2	0 (0.0)	3 (20.0)	3 (10.0)
3	3 (20.0)	0 (0.0)	3 (10.0)
Hyperuricemic, n (%)[a]			
Yes	8 (53.3)	5 (33.3)	13 (43.3)
No	7 (46.7)	10 (66.7)	17 (56.7)
Diagnosis, n (%)			
Malignant lymphoma	6 (40.0)	2 (13.3)	8 (26.7)
Acute leukemia	9 (60.0)	13 (86.7)	22 (73.3)

ECOG Eastern Cooperative Oncology Group

[a] Defined as uric acid >7.5 mg/dL in patients ≥13 years or uric acid >6.5 mg/dL in patients <13 years at baseline

3.2 Administration of rasburicase

Twenty-nine of 30 patients completed days 1–5 of treatment; one patient in the rasburicase 0.20 mg/kg group withdrew from the study on day 1 after the first administration of rasburicase due to the lack of WBC count at baseline. Another patient (0.15 mg/kg group) completed 5 days of treatment but withdrew from the study on day 8 to avoid life-threatening complications due to three concomitant grade 4 AEs (cerebral hemorrhage, brain edema, and brain herniation). Fifteen patients in the 0.15 mg/kg group and 14 patients in the 0.20 mg/kg group were therefore evaluable for response.

3.3 Efficacy

The overall RR for all patients was 96.6% (95% CI 82.2–99.9%) (Table 2). The RR was slightly higher in the rasburicase 0.20 mg/kg group than in the 0.15 mg/kg group (100% [95% CI 76.8–100.0%] vs. 93.3% [95% CI 68.1–99.8%]).

RRs for patients with hyperuricemia at baseline were 87.5 and 100.0% in the rasburicase 0.15 and 0.20 mg/kg groups, respectively (Table 2).

Mean plasma uric acid concentrations by dose of rasburicase over time are presented in Fig. 1. Rasburicase produced a rapid decrease in plasma uric acid concentrations in both dose groups. Uric acid levels remained low throughout treatment in all patients except one non-responder in the 0.15 mg/kg group. Uric acid levels declined rapidly within 4 h of the first rasburicase dose in both dose groups and remained low up to 120 h after the first administration of rasburicase (Fig. 1). Mean plasma uric acid concentrations were reduced by 84.8% (95% CI 76.7–92.9%) and 92.9% (95% CI 88.7–97.0%) compared with baseline at 4 h after the first rasburicase administration for the 0.15 and 0.20 mg/kg groups, respectively. Reductions in the level of plasma uric acid were similar between the two groups at 24 h after the last administration of rasburicase on day 6 (approximately 88%).

3.4 Safety

Owing to the severity of the underlying disease, all patients experienced at least one grade 3/4 AE, regardless of rasburicase treatment. The most common grade 3/4 AEs were leukopenia (86.7% of patients), neutropenia (83.3%), lymphocytopenia (80.0%), and increased ALT levels